Science of the Total Environment 794 (2021) 148365

Contents lists available at ScienceDirect

Science of the Total Environment

journal homepage: www.elsevier.com/locate/scitotenv

Mass absorption cross-section and absorption enhancement from long term black and elemental carbon measurements: A rural background station in Central Europe

Saliou Mbengue [a,*], Nadezda Zikova [b], Jaroslav Schwarz [b], Petr Vodička [b], Adéla Holubová Šmejkalová [c,d], Ivan Holoubek [a,e]

[a] Global Change Research Institute of the CAS, Brno 603 00, Czech Republic
[b] Institute of Chemical Process Fundamentals of the CAS, Prague 180 00, Czech Republic
[c] Czech Hydrometeorological Institute, Košetice Observatory, Košetice 394 22, Czech Republic
[d] Institute for Environmental Studies, Faculty of Science, Charles University, Prague 128 01, Czech Republic
[e] RECETOX, Masaryk University, Brno 625 00, Czech Republic

HIGHLIGHTS

- 5-Years field measurement of MAC_{eBC} and E_{abs} conducted at a rural background site
- Different approaches used to estimate E_{abs} and BrC coatings attributed absorption
- Temporal trend of MAC_{eBC} depending on the wavelength contrarily to B_{abs}
- Contribution of BrC coatings estimated up to 40% of the total absorption
- Increased E_{abs_660} due to relatively larger coating on aged PM during summer

GRAPHICAL ABSTRACT

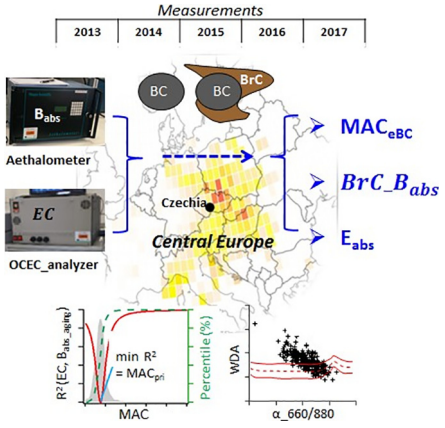

ARTICLE INFO

Article history:
Received 24 March 2021
Received in revised form 24 May 2021
Accepted 6 June 2021
Available online 16 June 2021

Editor: Pingqing Fu

Keywords:
Aerosol light absorption
Black carbon
Elemental carbon
Brown carbon
MAC
Absorption enhancement

ABSTRACT

Black carbon (BC) is a dominant aerosol light absorber, and its brown carbon (BrC) coating can enhance absorption and lead to uncertainties concerning the radiative forcing estimation. This study investigates the mass absorption cross-section of equivalent BC (MAC_{eBC}) during a long-term field measurement (2013–2017) at a rural Central European site. The MAC enhancement factor (E_{abs}) and the contribution of BrC coatings to the absorption coefficient (B_{abs}) were estimated by combining different approaches. The annual mean B_{abs} and MAC_{eBC} values decreased slightly over the measurement period associated with change in the submicron aerosol size distribution. Regardless of the wavelength, B_{abs} exhibited clear seasonal and diurnal variations, with higher values in winter when a higher absorption Ångström exponent (1.4) was observed due to the local biomass burning (BB). In contrast, MAC_{eBC} did not have a distinct temporal trend at 600 nm (7.84 ± 2.79 m^2 g^{-1}), while it showed a seasonal trend at 370 nm with higher values in winter (15.64 ± 4.77 m^2 g^{-1}). During this season, E_{abs_660} was 1.18 ± 0.27 and did not exhibit any clear wavelength dependence, despite the influence of BB. During the study period, BrC-attributed absorption was observed in 31% of the samples, with a contribution of up to 40% of total B_{abs}. In summer, the E_{abs_660} increased to 1.59 ± 0.60, when a larger BC coating could be formed by secondary aerosol fractions. During this season, MAC_{eBC_660} and E_{abs_660} showed comparable source profiles that

* Corresponding author.
E-mail address: mbengue.s@czechglobe.cz (S. Mbengue).

https://doi.org/10.1016/j.scitotenv.2021.148365

were mainly associated with aged air masses over central Europe, thereby supporting the fact that characteristics of coating materials formed during atmospheric aging are a major factor driving the MAC_{eBC_660} measured at the regional background site. Further field investigations of the composition of BC coatings would help to better understand and estimate uncertainties related to the radiative effect of aerosols.

1. Introduction

Black carbon (BC) is ubiquitous in the atmosphere and represents a minor fraction (less than 10%) of the total mass concentration of atmospheric aerosol ($PM_{2.5}$ and PM_{10}) (Putaud et al., 2004; Yttri et al., 2007). It is a primary carbonaceous aerosol fraction generated during the incomplete combustion of fossil fuels and biomass (Bond et al., 2013). Externally or internally mixed BC can be emitted by combustion sources, whereas internally mixed BC can also be formed during atmospheric transport through aging processes such as condensation and/or coagulation (Bond et al., 2013; Liousse et al., 1993; Zanatta et al., 2016).

BC is the main light-absorbing aerosol component and ranks second among climate forcing agents after carbon dioxide, with a total climate forcing of $+1.1$ W m^{-2} (Bond et al., 2013). In addition to BC, organic aerosols and mineral dust can absorb light (Bond et al., 2013; Leskinen et al., 2020; Wang et al., 2016). Certain dark organic aerosols called brown carbon (BrC) can significantly contribute (up to nearly half) to the light absorption by carbonaceous aerosols (Feng et al., 2013; Wang et al., 2016), especially at the ultraviolet (UV) wavelengths (Andreae and Gelencsér, 2006; Bond et al., 2013; Kirchstetter et al., 2004). This brown carbonaceous fraction is mainly emitted during biomass burning (BB) or biofuel combustion, but it can also be formed through the atmospheric photooxidation of reactive volatile organic compounds (VOCs) and gas-to-particle conversion (Lee et al., 2014; Wang et al., 2016 and reference therein). Different methods have been used to measure BrC-attributed absorption. Due to the variability of sources, chemical transformations, and optical properties of BrC, uncertainty in separating BrC absorption from BC absorption leads to significant uncertainties concerning the estimates of radiative forcing (Bond et al., 2013; Wang et al., 2016). Traditionally, the direct estimation of BrC absorption has been performed with offline aerosol collection and laboratory extraction of samples in water and organic solvents (Cappa et al., 2019; Cheng et al., 2017; Kirchstetter et al., 2004; Kirillova et al., 2016; Washenfelder et al., 2015). However, this method is time-consuming and has limitations, especially for long-term and high-resolution field measurement campaigns (Cheng et al., 2021; Wang et al., 2016). Indirect methods for the estimation of BrC-attributed absorption have been developed using multiple wavelengths (from UV to near-infrared) to measure absorption coefficients (Chow et al., 2018; Kirchstetter et al., 2004; Wang et al., 2016). Recently, Wang et al. (2016) developed the Wavelength Dependence of Absorption Ångström Exponent (WDA) method to estimate the contribution of BrC to light absorption. Considering the wavelength dependence of the wavelength dependence of light absorption, this approach combines the calculated Ångström exponent (α) for two wavelength pairs from ambient air measurements (aethalometer AE31 in this case) and Mie calculations, to predict the existence of BrC absorbers in ambient particles (Leskinen et al., 2020; Wang et al., 2016).

The mass absorption cross section (MAC) of BC (MAC_{BC}) defines the relationship between its atmospheric concentrations and direct radiative forcing (DRF) due to BC. This is a fundamental input to models of radiative transfer (Wang et al., 2016).

MAC_{BC} depends on the different chemical and microphysical properties of the particles, including particle size and shape, refractive index, density, and the mixing state of BC (Bond et al., 2013). A MAC_{BC} of 7.5 ± 1.2 m^2 g^{-1} at 550 nm suggested by Bond and Bergstrom (2006) was widely used for freshly emitted BC. An internal mixture of BC and other aerosol chemical components, however, may generally result in enhanced light absorption through the lensing effect (Bond et al., 2013; Zanatta et al., 2016), leading to uncertainties in the modeling of the radiative forcing of BC (Bond et al., 2013).

B_{abs_pri} is generally determined by removing the coating material on BC and measuring the absorption coefficient of the uncoated fraction. The coating material on BC can be removed with an aerosol filter filtration dissolution (AFD) analogue to estimate BrC absorption, or by the use of a thermal denuder (TD, 200–300 °C) upstream of the instrument (Cappa et al., 2019 and references therein; Lack et al., 2012; Yuan et al., 2020) and detection with a photoacoustic spectrometer (PAS).

When using MAC, the determination of MAC_{pri} is a fundamental parameter in the estimation of E_{abs} (Eq. (4)). One approach is to adopt the reference MAC_{pri} based on the literature, but these values are variable depending on the location, sources, and measurement period, and may not be representative of MAC_{pri} for a given site. Another approach is to determine MAC_{pri} based on a correlation analysis of the concurrent measurements of both MAC_{BC} and BC particle mixing state with a single-particle soot photometer (SP2) or soot particle aerosol mass spectrometer (SP-AMS) (Cappa et al., 2019; Sun et al., 2020; Yuan et al., 2020).

The TD-PAS, SP2, and SP-AMS methods have the advantage of providing high time resolution data, but the high cost of these systems reduces their worldwide field deployment, particularly for long-term measurements (Sun et al., 2020; Wu et al., 2018). Wu et al. (2018) recently developed an alternative new statistical approach. It consists of applying the minimum R squared (MRS) in the well-known EC tracer method. The concept of dissociating B_{abs} into B_{abs_pri} and B_{abs_aging} is analogous to the dissociation of OC into primary OC (POC) and secondary (SOC) in the EC tracer method (Wu and Yu, 2016), and would enable a long-term E_{abs} calculation at more locations where the aethalometer and ECOC analyzer are deployed simultaneously.

Despite the importance of MAC_{eBC} in BC radiative forcing estimation, there are relatively few studies based on long-term measurements of MAC_{eBC} in rural background areas. The aim of this study is to characterize the eBC absorption properties, including MAC_{eBC}, at a rural background station by considering different time scales (yearly, seasonal, and diurnal variations) and different wavelengths based on a multiple-year measurement period. The estimation of the light absorption enhancement (E_{abs}) and the influence of BrC-attributed absorption are investigated by combining different approaches to estimate the effects of BC and BrC in the atmosphere.

2. Methodology

2.1. Measurement site

The study was conducted at the National Atmospheric Observatory Košetice (NAOK), a Central Europe rural and regional background site that is located in the Bohemian-Moravian Highlands, the Czech Republic. It is at 49°35′N, 15°05′E and 534 m above sea level (ASL) (Fig. 1). NOAK has been involved in various national and international monitoring programs, including the Aerosol, Clouds, and Trace Gases Research Infrastructure Network (ACTRIS) and its Czech version ACTRIS_CZ, the Integrated Carbon Observation System (ICOS), the Global Mercury Observation System (GMOS), the European Monitoring and Evaluation Programme (EMEP), the Global Atmosphere Watch (GAW), and the Czech Air Quality Information System (ISKO) databases.

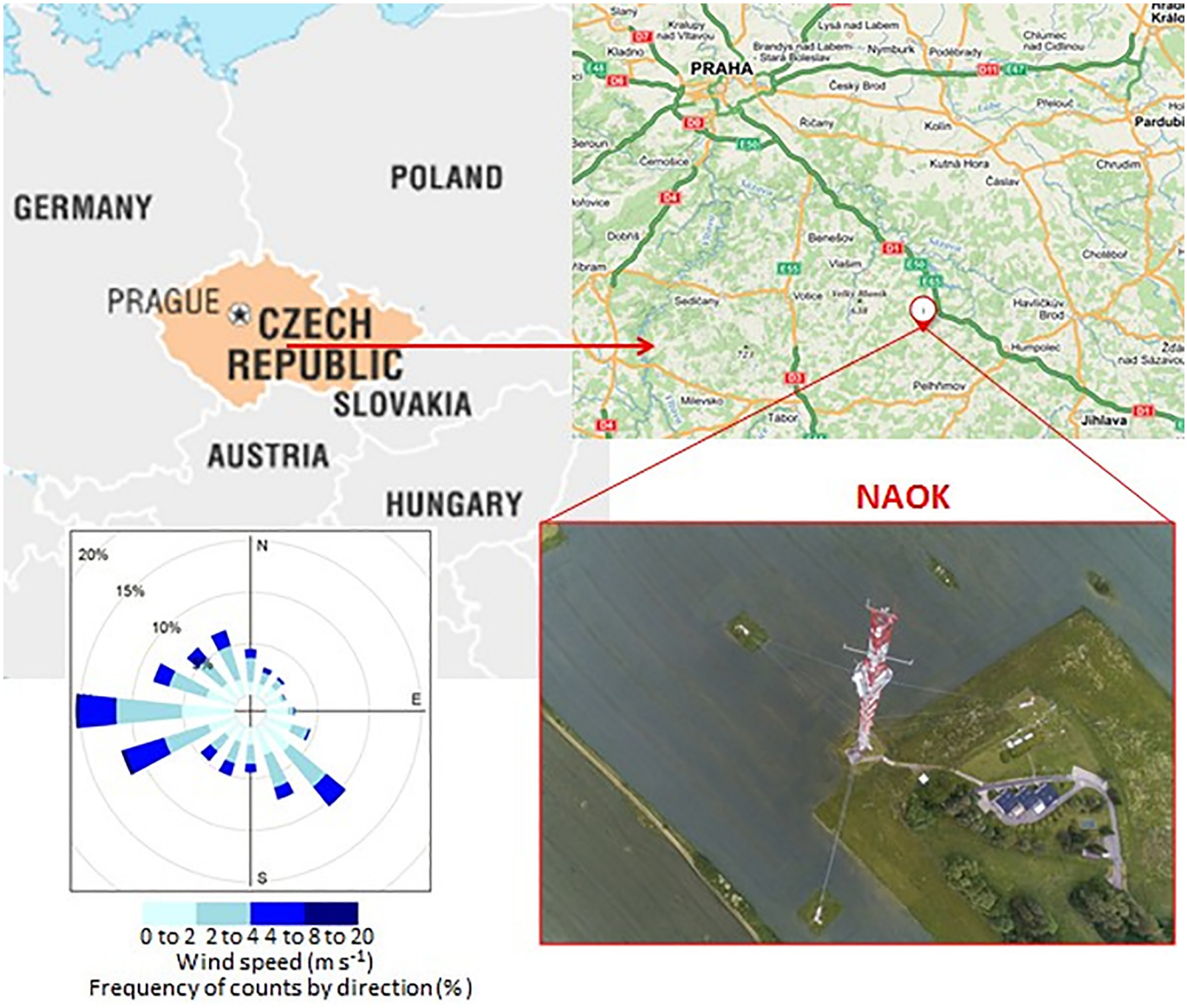

Fig. 1. Location of the National Atmospheric Observatory Košetice (NAOK) and prevailing wind direction (hourly average of during the measurements campaign).

The station is surrounded by an agricultural landscape and several village settlements with a couple of hundred inhabitants, and is approximately 70 km southeast of the urban area of Prague (population of 1,300,000, CSO, 2021). The closest main road is located approximately 1 km east of the sampling station, and one of the major Czech highways (40,756 cars/day, CSD, 2016) is approximately 6 km north and northeast. NAOK is affected by regional and long distance transported air masses, mainly associated with western and southeastern winds (Dvorská et al., 2015; Mbengue et al., 2020, 2018; Schwarz et al., 2016; Vodička et al., 2015; Zíková and Ždímal, 2013).

2.2. Light absorption measurements

Measurements of the absorption coefficient (B_{abs}) were conducted from March 2013 to December 2017 at NAOK. The B_{abs} was measured with a multiwavelength aethalometer (Model AE31, Magee Scientific, Berkeley, CA, USA, Hansen, 2005) at seven wavelengths (370, 470, 520, 590, 660, 880, and 950 nm). The airborne particles were sampled at 4 m above the ground with a PM_{10} sampling head (Leckel GmbH) on the roof of the measurement container, and the sampling system was equipped with a sample dryer (custom-made Nafion dryer, TROPOS, Leipzig, Germany). The instrument was operated at a flow rate of 4 L min^{-1} with a 5-min interval sampling time. All data were processed and evaluated according to the EMEP standard operating procedure.

For filter-based absorption measurement techniques, different correction methods have been developed to minimize the uncertainties from artifacts caused by loading, matrix, and scattering effects (Arnott et al., 2005; Collaud Coen et al., 2010; Müller et al., 2011; Schmid et al., 2006; Virkkula et al., 2007; Weingartner et al., 2003; WMO, 2016; Zanatta et al., 2016). In this study, the correction for filter-loading (Virkkula et al., 2007) and multiple-scattering effects (correction factor C: 3.5) were applied according to the recommendation based on the intercomparison of parallel aethalometer and MAAP measurements of atmospheric aerosols (WMO, 2016; Zanatta et al., 2016). In addition to these corrections, data points recorded at a relative humidity (RH) of above 40% were omitted to limit the uncertainties induced by the hygroscopic growth of particles (Mbengue et al., 2020; Wu et al., 2018).

2.3. OC and EC measurements

The mass concentrations of EC and OC were measured from March 2013 to December 2017 using a semi-continuous thermal-optical

organic/elemental carbon analyzer (Sunset Laboratories model 4) in accordance with the shortened EUSAAR-2 protocol (Cavalli et al., 2010; Karanasiou et al., 2020). The measurement method is detailed in a previous study (Mbengue et al., 2018). After being placed in the same container as the AE31, the OCEC analyzer was sampled every 4 h (including 20 min of OC/EC thermo-optical analysis) at a flow rate of 8.0 L min^{-1} through a $PM_{2.5}$ cyclone inlet at 4 m above the ground. To prevent positive artifacts because of the absorption of volatile organic compounds on the quartz fiber filter (Turpin et al., 2000), the sampling line was equipped with a carbon parallel-plate diffusion denuder (Sunset Lab).

2.4. MAC and E_{abs} estimation

MAC_{BC} describes the absorption efficiency per mass of BC and it can be used to convert the mass concentrations of equivalent BC (*eBC*, that is, the mass of BC determined by an optical method) to their light-absorption coefficients (B_{abs}) at a given wavelength (λ) according to Eq. (1):

$$eBC_{\lambda} = \frac{B_{abs\_\lambda}}{MAC_{eBC\_\lambda}} \quad (1)$$

Isolating BC from other aerosol light absorbers is very challenging, and a direct method for measuring BC mass concentration without interference is lacking (Baumgardner et al., 2012; Pileci et al., 2021). To determine MAC_{eBC}, the mass concentration of elemental carbon (*EC*) measured by thermo-optical methods was used as *eBC* despite their different operational definitions (Bond and Bergstrom, 2006; Karanasiou et al., 2020; Petzold et al., 2013). Therefore, MAC_{eBC} was estimated using B_{abs} measured by filter-based optical methods divided by *EC* concentration (Baumgardner et al., 2012; Bond et al., 2013; Cheng et al., 2011; Cho et al., 2019; Knox et al., 2009; Zanatta et al., 2016), as shown in Eq. (2):

$$MAC_{eBC\_\lambda} = \frac{B_{abs\_\lambda}}{EC} \quad (2)$$

The specific absorption cross-section of particulate matter (MAC_{PM_λ}) can also be obtained from the ratio between B_{abs_λ} of eBC and the mass concentration of PM (Knox et al., 2009), as in Eq. (3):

$$MAC_{PM\_\lambda} = \frac{B_{abs\_\lambda}}{PM} \quad (3)$$

The light absorption enhancement (E_{abs_λ}) can be calculated by dividing the total B_{abs_λ} or MAC_{eBC_λ} by their primary fractions ($B_{abs\_pri\_\lambda}$ and MAC_{pri_λ}) as in Eq. (4) (Sun et al., 2020; Wu et al., 2018):

$$E_{abs\_\lambda} = \frac{B_{abs\_\lambda}}{B_{abs\_pri\_\lambda}} = \frac{MACeBC\_\lambda}{MAC_{pri\_}\lambda} \quad (4)$$

where $B_{abs\_pri\ \lambda}$ and $MAC_{pri\ \lambda}$ are the primary or reference B_{abs} and MAC, respectively, measured at wavelength λ for freshly emitted BC particles. In this study, the E_{abs_λ} was calculated as the ratio between MAC_{λ} and MAC_{pri_λ} according to Eq. (4). MAC_{pri} was estimated by applying the minimum R squared (MRS) in the EC tracer method consisting of dissociating B_{abs} into B_{abs_pri} and B_{abs_aging} as for OC into POC and SOC, with MAC_{pri} corresponding to the primary OC/EC ratio ($[OC/EC]_{pri}$) (Eqs. (5) and (6)) (Wu and Yu, 2016; Wu et al., 2018):

$$B_{abs\_\lambda} = B_{abs\_pri\_\lambda} + B_{abs\_aging\_\lambda} \quad \sim \quad OC = \mathrm{POC} + \mathrm{SOC} \quad (5)$$

$$B_{abs\_pri\_\lambda} = MAC_{pri\_\lambda} \times EC \quad \sim \quad \mathrm{POC} = [\mathrm{OC/EC}]_{pri} \times EC \quad (6)$$

The MRS method estimates the primary ratios (e.g., $[OC/EC]_{pri}$, MAE_{pri}) by investigating the inherent independence between a primary pollutant (e.g., EC) and a secondary component (e.g., SOC, B_{abs_aging}) during atmospheric aging (Sun et al., 2020; Wu et al., 2018; Wu and Yu, 2016). A description of the MRS method has been detailed in Wu et al. (2018), and a computer program was built in Igor Pro (WaveMetrics, Inc. Lake Oswego, OR, USA) for its easy application (Wu, 2017a). The EC from the thermo-optical analyzer and 4-hours mean B_{abs} from AE31 are used as input variables. The correlation between EC and B_{abs_aging} was examined and the MAC obtained at the minimum R^2 was taken as MAC_{pri}. Assuming that MAC_{pri} varies continuously in a reasonable range of 0.1 to 50 $m^2\ g^{-1}$, a series of R^2 (between EC and B_{abs_aging}) values can be plotted against the desired MAC_{pri} (Fig. 2). Considered as a primary light absorption due to soot particles, B_{abs_pri} is well correlated with the EC mass. Inversely, B_{abs_aging}, due to the coating of particles formed during atmospheric transport and its variability, depends on the coating thickness, independently of the EC mass. As a result, the minimum R^2 (between EC and B_{abs_aging}) would correspond to the best MAC_{pri} of the dataset representing the overall MAC_{pri} from different primary emission sources instead of MAC_{pri} from a single primary source as for ($[OC/EC]_{pri}$) in the EC tracer method (Wu et al., 2018; Sun et al., 2020).

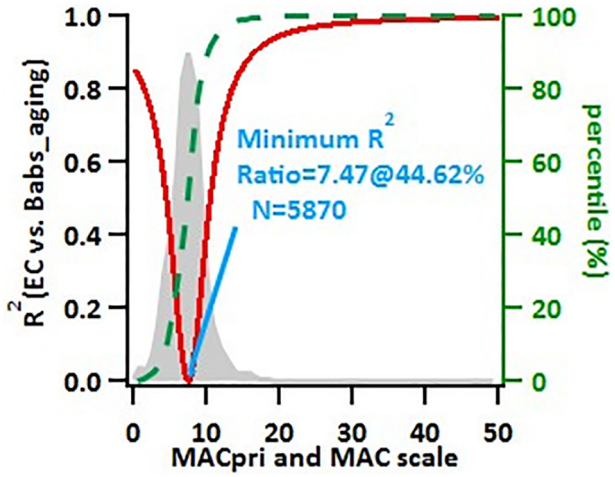

Fig. 2. Example of a MRS plot for the MAE_{pri} estimation at 660 nm showing the frequency distribution of the observed MAC (grey area), the cumulative distribution of MAC (dashed green line) and the R^2 obtained from the correlation between EC mass and B_{abs_aging} (red curve).

Notably, the estimated E_{abs} with the MRS is not affected by systematic MAC bias due to EC variability and B_{abs} overestimation (Wu et al., 2018). In the latter study, the performance of the MRS approach was investigated in response to the systematic MAC bias during a 1-year measurement campaign at a suburban site in the Pearl River Delta region of China, with EC concentrations four times higher (2.66 ± 2.27 μg m^{-3}) than those measured at NAOK (Mbengue et al., 2018). Only a small effect of EC variability and B_{abs} overestimation on the E_{abs} estimation was found (Wu et al., 2018). In the present study, however, the MAC_{pri_660} estimation by the MRS approach was found to be sensitive to fluctuations in the measured EC. The frequency distribution of ambient EC was examined for model parameterization for the present site (Fig. S1), and outliers in the data ($n = 20$, 0.3%) were identified and excluded from the dataset. The comparison of MAC_{pri_660} before, and after, the treatment shows that the non-clearance of the outliers can lead to a MAC_{pri_660} decrease by a factor up to 2 (Fig. S2a, b), resulting in an overestimation of E_{abs_660}, particularly in summer (August).

2.5. Estimation of the secondary organic carbon (SOC)

The EC tracer method has been widely used to estimate the SOC contribution to the total OC concentration. As stated in Eq. (6), the determination of $[OC/EC]_{pri}$ is crucial for the estimation of SOC. Classical approaches for determining $[OC/EC]_{pri}$ include the use of a minimum OC/EC ratio during a study period, or the lowest measured OC/EC ratios,

ambient OC and EC concentrations dominated by the influence of primary source emissions, and atmospheric concentrations of OC and EC at times when little photochemical activity occurred (Cabada et al., 2004; Castro et al., 1999; Pio et al., 2011; Strader et al., 1999; Turpin and Huntzicker, 1995, 1991; Wu and Yu, 2016).

In this study, MRS was applied to estimate $[OC/EC]_{pri}$ using EC and OC as input variables (Wu and Yu, 2016). Similar to MAC_{pri}, an Igor Pro-based computer program (WaveMetrics, Inc. Lake Oswego, OR, USA) (Wu, 2017b) was used for the MRS estimation of $[OC/EC]_{pri}$ and SOC. As for MAC_{pri}, the correlation (R^2) between measured EC and estimated SOC was investigated assuming a series of hypothetical $[OC/EC]_{pri}$ values varying from 0.1 to 10. Considering the independency between EC and SOC, the minimum R^2 (between EC and SOC) would correspond to the best $[OC/EC]_{pri}$ of the dataset.

In Mbengue et al. (2018), $[OC/EC]_{pri}$ of 1.89 in summer was estimated by inspecting OC versus EC scatter plots (Pio et al., 2011) using the 20% lowest measured OC/EC ratios under low photochemical activity (between 06.00 and 10.00 UTC). For comparison, the MRS method was applied to the summer data during the morning period between 6:00 and 10:00 (Fig. S3). The estimated $[OC/EC]_{pri}$ by the MRS method (1.74) was consistent with the previous estimate using the lowest 20% measured OC/EC ratios (difference < 10%). Therefore, the MRS method can be used for $[OC/EC]_{pri}$ estimation at the rural background site.

2.6. BrC absorption estimation

2.6.1. WDA method and Mie-modeled absorption Ångström exponent

The absorption Ångström exponent (α) is generally used to describe the spectral dependence of light absorption (Bond et al., 2013; Harrison et al., 2013; Kirchstetter et al., 2004; Sandradewi et al., 2008; Vaishya et al., 2017) and it can also provide insight regarding the potential sources of BC. α can be calculated as follows:

$$\alpha\_370/880 = -\frac{\log\left(\frac{B_{abs\_370}}{B_{abs\_880}}\right)}{\log\left(\frac{370}{880}\right)} \quad (7)$$

The contribution of BrC to the absorption coefficient using the WDA method is estimated by comparing α calculated using the AE31 measurements and those estimated by Mie calculations (Leskinen et al., 2020; Wang et al., 2016). In this study, α was calculated for the 370 and 880 nm (α_370/880) and 660 and 880 nm (α_660/880) wavelength pairs, and the WDA referred to Δα_λ was determined as in Eq. 8 (Wang et al., 2016):

$$\Delta\alpha\_\lambda = \alpha\_370/880 - \alpha\_660/880 \quad (8)$$

The Δα_λ values for each observation were compared with the Δα_λ values calculated using the Mie simulation. The Mie calculations were performed using a computer program written in Igor Pro (WaveMetrics, Inc. Lake Oswego, OR, USA) (Wu, 2017b; Wu et al., 2018). The model simulation was simplified by assuming a constant density for spherical particles and both core diameters (D_{core}) and shell diameters (D_{shell}) constrained in the range of 10–3000 nm (Wu et al., 2018). The Mie simulation was performed adopting a core-shell model which more represents the reality (coating due to the aging process), with the refractive index (RI) of 1.85–0.71 for soot core and 1.55 for the coating material (Wu et al., 2018).

For particles smaller than 200 nm, the modeled α_660/880 varied from 1 to 1.3, which is consistent with the reported values for BC particles close to unity (Kirchstetter et al., 2004; Sandradewi et al., 2008; Vaishya et al., 2017). For particles >200 nm, α_660/880 decreased significantly, showing a strong size dependence of α for larger particles (Fig. S4). In addition, other RI values were modeled, with similar results regarding the dependence of α_660/880 on α for particles over 100–200 nm (Fig. S5).

2.6.2. Ångström exponent law

When measuring with a multiwavelength aethalometer, the light absorption measured at the near-infrared wavelength region (880 nm) is mainly attributed to BC if dust is absent (Leskinen et al., 2020). Knowing the α for BC, its contribution to the absorption coefficient at shorter wavelength (370 nm) can be calculated using the Ångström exponent law (Eqs. (9) and (10)) (Leskinen et al., 2020):

$$\frac{B_{abs_{370\_eBC}}}{B_{abs_{880\_eBC}}} = \left(\frac{370}{880}\right)^{-\alpha_{eBC}} \quad (9)$$

$$B_{abs_{370\_eBC}} = B_{abs_{880\_eBC}} \times \left(\frac{370}{880}\right)^{-\alpha_{eBC}} = B_{abs_{880}} \times \left(\frac{370}{880}\right)^{-\alpha_{eBC}} \quad (10)$$

The Ångström exponent of unity has been widely adopted in the literature for BC particles (Kirchstetter et al., 2004; Sandradewi et al., 2008; Vaishya et al., 2017). However, using a fixed value for the α_{eBC} may not reflect α for ambient-coated or internally mixed BC particles, which may be influenced by particle characteristics, including particle size (Fig. S4) and chemical composition (Kirchstetter et al., 2004; Lack and Langridge, 2013; Wang et al., 2016). Consequently, the use of $\alpha = 1$ for eBC may lead to an underestimated or overestimated $B_{abs_{370\_BrC}}$.

In this study, B_{abs370_eBC} (Eq. (10)) was estimated by comparing this traditional method ($\alpha_{eBC} = 1$) with the method of Wang et al. (2016) using the lowest and the highest Δα_λ for the estimation of the α_370/880 as in Eq. (11):

$$\alpha\_370/880 = \alpha\_660/880 - \Delta\alpha\_\lambda \quad (11)$$

The contribution of BrC to light absorption can be obtained by subtracting $B_{abs_{370\_eBC}}$ calculated in Eq. (10) from the measured absorption coefficient by the aethalometer at 370 nm ($B_{abs_{370}}$) as follows:

$$B_{abs_{370\_BrC}} = B_{abs_{370}} - B_{abs_{370\_BC}} \quad (12)$$

and the relative contribution of BrC to the $B_{abs_{370}}$ can be calculated as the ratio between $B_{abs_{370\_BrC}}$ and $B_{abs_{370}}$.

2.7. Source area analysis

The geographical origins of local and distant sources affecting the NAOK receptor site and their contributions have been explored by combining the conditional bivariate probability function (CBPF) and potential source contribution function (PSCF) analyses.

A CBPF polar plot shows the variation of a pollutant concentration in relation to wind speed and wind direction. It allows the identification of the direction in which potential sources are located and the transport characteristics of pollutants (Uria-Tellaetxe and Carslaw, 2014). In this study, a CBPF analysis (Uria-Tellaetxe and Carslaw, 2014) was performed using the openair package (Carslaw and Ropkins, 2012) in R (R Core Team, 2020). For the calculation, the 75th percentile was used as a threshold, so in the CBPF, the probability of the concentration between the 75th and 100th percentiles was calculated for wind speed and direction in each season.

The PSCF calculates the conditional probabilities to assess the contribution of a geographical location of the potential sources affecting the receptor site. For the PSCF analysis, 72-h air mass back trajectories arriving at 100 m above ground level (AGL) were calculated every 6 h using the HYSPLIT_4 model (Rolph et al., 2017; Stein et al., 2015) and meteorological data from the Global Data Assimilation System (GDAS) archive information with a resolution of 1° × 1°. For the PSCF calculation, the split and openair R packages were used. For the PSCF, the 75th percentile was also used as a threshold, and weighting with the 20 data points set as the minimum in each grid cell was applied (Zíková et al., 2016). The PSCF, as well as the gridded difference was plotted, and the difference compared the percentage of air masses in a grid point for all data to a subset of data with a concentration over the 90th percentile.

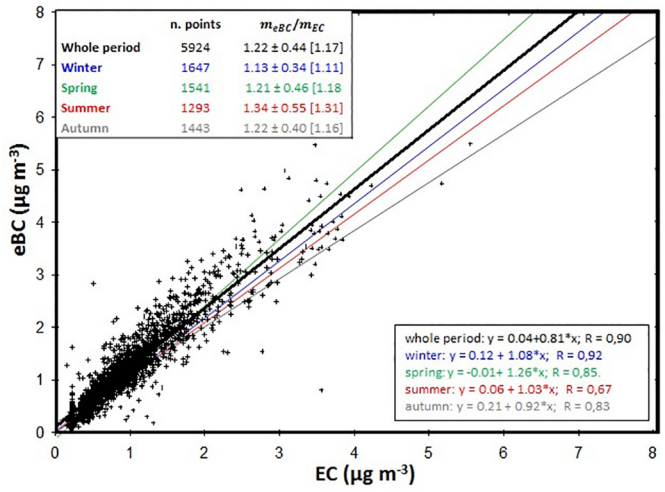

Fig. 3. Correlation between eBC in PM_{10} and EC in $PM_{2.5}$ measured at the NAOK during the whole period and for different seasons. The insert table shows eBC to EC ratio for different seasons: mean (±std) and median (in brackets). p = 0.000 for all seasons.

2.8. Auxiliary measurements

Additional measurements were also performed at the station during the campaign (Table S1), including meteorological parameters (temperature, wind speed, and direction), PM_{10} concentration (by radiometry-beta ray absorption), particle number size distribution (scanning mobility particle sizer, SMPS, TROPOS, Leipzig, Germany), trace gases such as NO_2 and NO_x (chemiluminescence), SO_2 (UV-photometric), and CO (IR abs. spectrometry).

From the data, the temporal trend was estimated using the TheilSen function within the openair package (Carslaw and Ropkins, 2012). For the calculations, the de-seasoned version of the test was applied on the daily averages of absorption parameters, $PM_{2.5}$ and PM_{10} concentrations as well as on the SMPS data (total number, volume, and mass concentration in the size range 10–800 nm).

3. Results and discussion

3.1. EC in $PM_{2.5}$ vs eBC in PM_{10}

At NAOK from 2013 to 2017, *eBC* in PM_{10} correlated well with *EC* in $PM_{2.5}$ (R = 0.90) and the concentrations are comparable with the mean (±std) *eBC/EC* ratio of 1.22 ± 0.44 for the entire period ranging from 1.13 ± 0.34 to 1.34 ± 0.55 in individual seasons (Fig. 3). The relatively lower correlation between measured eBC and EC in summer might be due to the lower EC measured in summer (Mbengue et al., 2018), but also to the influence of BrC attributed absorption (Sections 3.3 and 3.4).

There was no significant difference between the measured *EC* in $PM_{2.5}$ and *eBC* in PM_{10} ($p < 0.05$) at NAOK. This result suggests that there should be no significant difference between B_{abs} of eBC in both size fractions ($PM_{2.5}$ and PM_{10}), even though the measured size cutoffs between the Sunset EC/OC analyzer and the aethalometer differ. Consequently, *EC* can be taken as a representative of *eBC* and for the purpose of this study, and it can be used for the determination of MAC_{eBC} according to Eq. (2). Notably, BC is exclusively associated with fine particles, while the coarse fraction is dominated by mineral dust (Clarke et al., 2004) which may scatter light, leading to an overestimation of light absorption (Leskinen et al., 2020). This approach has previously been used by Zanatta et al. (2016), who used B_{abs} and *EC* measured in different size fractions of PM to estimate MAC_{eBC} at different European regional background sites of the ACTRIS network (Aerosols, Clouds, and Trace Gases Research InfraStructure; http://www.actris.eu).

3.2. Temporal characteristics of absorption properties

3.2.1. Inter-annual variability

The overall mean B_{abs}, MAC_{PM}, and MAC_{eBC} measured at 660 nm at NAOK were 4.74 ± 3.97 Mm^{-1}, 0.50 ± 0.27 $m^2\ g^{-1}$ and 7.84 ± 2.79 $m^2\ g^{-1}$, respectively. The annual mean values decrease slightly over the five years (Table 1) (Table S2). When comparing the overall mean B_{abs_660}, MAC_{PM_660}, and MAC_{eBC_660} values to individual years, a statistically significant ($p < 0.05$) decreasing trend was found using the TheilSen function. A further statistically significant ($p < 0.05$) trend was found in $PM_{2.5}$ and in total volume concentrations of atmospheric aerosol particles in the size range from 10 to 800 nm, and in contrast, no trend was found in EC, OC, and PM_{10} concentrations. Therefore, the changes in absorption properties can be linked to changes in the size distribution of fine aerosol particularly in the submicron fraction, rather than to the total mass or composition.

B_{abs_660} measured at NAOK falls within the range of 3.7 to 11 Mm^{-1} measured at 637 nm in different Central Europe background sites and British Isles (Zanatta et al., 2016). These authors also observed lower values in southern Scandinavia (0.66 to 1.3 Mm^{-1}) and in the Mediterranean (2.3 to 2.8 Mm^{-1}). Wu et al. (2018) found a significantly higher B_{abs_550} value (42.65 ± 30.78 Mm^{-1}) in polluted areas in the Pearl River Delta.

MAC_{eBC} observed in previous studies conducted at different backgrounds and remote sites was also compared (Fig. 4) (Table S3). The overall MAC_{eBC} at NAOK varied from 4.78 ± 1.91 $m^2\ g^{-1}$ (at 950 nm) to 12.15 ± 4.05 $m^2\ g^{-1}$ (at 370 nm) (Table S3). MAC_{eBC} measured at 660 nm and 590 nm were in the range of 7.5 to 13.3 $m^2\ g^{-1}$ measured at a corresponding or close wavelength (637 nm) by Zanatta et al. (2016) during an extensive intercomparison and harmonization campaign at nine European regional background sites. Comparable MAC_{eBC_637} were also observed in Europe by Nordmann et al. (2013) and Pandolfi et al. (2014). Herich et al. (2011) reported significantly higher MAC_{eBC_660} (14.4 and 18.5 $m^2\ g^{-1}$) at two rural sites in Switzerland (Magadino and Payerne).

The values reported in the literature (Fig. 4) (Table S3) vary, which could be related to the influence of various factors, including differences in sources, chemical and microphysical properties of the particles, the

Table 1
Overall, annual and seasonal mean (±standard deviation) and median (in brackets) values measured at NAOK for B_{abs_660}, MAC_{eBC_660}, MAC_{PM}, PM_{10}, EC and OC concentrations.

	B_{abs_660} [Mm^{-1}]	MAC_{eBC_660} ($m^2\ g^{-1}$)	MAC_{PM_660} ($m^2\ g^{-1}$)	PM_{10} [µg m^{-3}]	*EC* [µg m^{-3}]	*OC* [µg m^{-3}]
Whole period	4.74 ± 3.97 (3.52)	7.84 ± 2.79 (7.77)	0.50 ± 0.27 (0.46)	17.35 ± 10.03 (14.79)	0.65 ± 0.52 (0.48)	2.86 ± 2.00 (2.36)
2013	5.88 ± 4.45 (4.67)	9.51 ± 3.59 (9.08)	0.61 ± 0.38 (0.57)	18.17 ± 8.94 (16.46)	0.63 ± 0.47 (0.49)	2.92 ± 1.80 (2.54)
2014	5.50 ± 4.50 (4.15)	8.33 ± 2.15 (8.13)	0.53 ± 0.23 (0.47)	18.52 ± 10.57 (15.75)	0.65 ± 0.60 (0.45)	2.91 ± 1.91 (2.46)
2015	4.26 ± 3.20 (3.30)	7.69 ± 2.23 (7.66)	0.47 ± 0.23 (0.41)	17.31 ± 9.01 (14.98)	0.71 ± 0.56 (0.56)	3.02 ± 2.19 (2.36)
2016	3.88 ± 3.20 (2.94)	6.65 ± 2.63 (6.36)	0.45 ± 0.25 (0.39)	16.40 ± 8.68 (14.42)	0.66 ± 0.46 (0.53)	2.61 ± 1.73 (2.20)
2017	4.31 ± 4.03 (2.77)	6.71 ± 2.28 (6.47)	0.47 ± 0.25 (0.45)	16.52 ± 12.24 (13.25)	0.58 ± 0.49 (0.40)	2.93 ± 2.43 (2.23)
Winter	4.74 ± 3.97 (3.52)	1.03 ± 1.10 (0.72)	0.50 ± 0.27 (0.46)	18.97 ± 14.05 (13.79)	0.88 ± 0.68 (0.70)	3.65 ± 2.65 (2.86)
Spring	6.46 ± 4.86 (5.38)	0.91 ± 0.78 (0.74)	0.65 ± 0.23 (0.61)	17.95 ± 9.59 (15.24)	0.63 ± 0.47 (0.48)	2.70 ± 1.89 (2.22)
Summer	4.87 ± 4.43 (3.43)	1.04 ± 0.70 (0.93)	0.46 ± 0.32 (0.43)	16.05 ± 6.77 (14.96)	0.34 ± 0.17 (0.26)	2.28 ± 1.11 (2.12)
Autumn	2.60 ± 1.37 (2.33)	0.79 ± 0.69 (0.56)	0.30 ± 0.11 (0.29)	16.65 ± 8.74 (14.79)	0.72 ± 0.49 (0.61)	2.80 ± 1.75 (2.46)

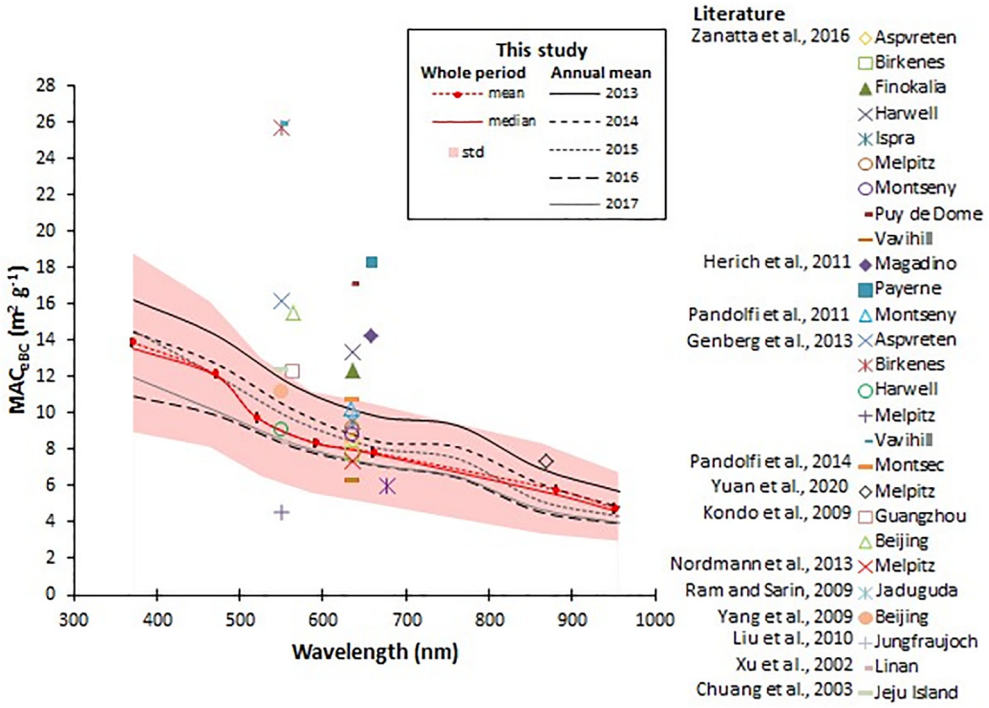

Fig. 4. Overall and annual mean MAC_{eBC} values estimated at the NAOK for different wavelengths in comparison to the reported values in the literature for different rural, regional background and remote sites.

mixing state of BC, atmospheric aging processes during transport of particles over a certain distance, and the techniques used to measure the BC mass concentration in each study (Bond et al., 2013; Genberg et al., 2013; Laborde et al., 2013; Liousse et al., 1993; Pandolfi et al., 2014, 2011; Yuan et al., 2020; Zanatta et al., 2016).

The MAC value (7.5 ± 1.2 $m^2\ g^{-1}$ at 550 nm) reported for freshly emitted or externally mixed BC (Bond and Bergstrom, 2006) is slightly lower than MAC_{eBC} observed at shorter wavelengths (520 and 590 nm) at NAOK (9.77 ± 3.29 $m^2\ g^{-1}$ and 8.36 ± 2.82 $m^2\ g^{-1}$, respectively). This might be related to the aging or coating of BC-containing particles, consistent with the characteristics of the NAOK rural background site that is affected by aged transported aerosols.

3.2.2. Seasonal and diurnal variation in B_{abs} and MAC_{eBC}

B_{abs_660} exhibited a clear seasonal trend with higher values during colder months and lower values during warmer periods (Fig. 5) (Table 1) (Table S4). The mean B_{abs_660} were two to three times higher in winter (6.46 ± 4.86 Mm^{-1}) than in summer (2.60 ± 1.37 Mm^{-1}). In spring and autumn, B_{abs_660} were 4.87 ± 4.43 Mm^{-1} and 5.16 ± 3.40 Mm^{-1}, respectively. Carbonaceous aerosols (OC and EC) and combustion-related trace gases (NO_x, SO_2, and CO) followed the same pattern as $B_{abs_}$660, with concentrations being higher in colder months (Fig. 5b, c), suggesting that they were affected by common sources and/or factors. A similar trend was previously observed by Zanatta et al. (2016) in Central Europe and Scandinavia, with higher B_{abs_637} and EC concentrations in winter and autumn, likely attributed to the increased emissions from heating, and lower planetary boundary layer height.

Season-dependent wavelength dependence of B_{abs} was also observed (Fig. 6a). B_{abs} increased at a shorter (370 nm) wavelength and exhibited a more pronounced seasonal variation with mean values ranging from 3.94 ± 2.04 Mm^{-1} in summer to 12.84 ± 9.34 Mm^{-1} in winter (Table S4). During the heating season, emissions from BB sources may contain a large fraction of organic compounds (Kirchstetter et al., 2004; Sandradewi et al., 2008) that may act as a coating of BC and lead to the enhancement of absorption, especially at shorter wavelengths (Bond et al., 2013; Kondo et al., 2009; Lack et al., 2012). During winter, BB tracers (levoglucosan and mannosan) showed higher concentrations at NAOK and were well correlated with eBC from BB (Mbengue et al., 2020). The monthly mean variation of estimated α was approximately 1 in summer and exhibited a higher value of 1.4 during the heating season (Fig. 5a) because BB emissions contributed significantly (approximately 50%) to the total eBC observed at NAOK (Mbengue et al., 2020).

The diurnal trend of B_{abs_660} was stronger in colder seasons (Fig. 6b) and exhibited a morning peak that was attributed to the morning traffic rush hour and an evening peak that was attributed to the concomitant effect of lower planetary boundary layer height and the influence of BB. MAC_{PM_660} followed similar seasonal (Figs. 5d and 6c) and diurnal (Fig. 6d) variations as B_{abs_660}, suggesting common sources or driving factors.

In contrast to B_{abs} and MAC_{PM}, MAC_{eBC} did not exhibit any distinct seasonal (Figs. 5d and 6e) and diurnal (Fig. 6f) trends at 660 nm. MAC_{eBC_660} was 7.76 ± 2.09 $m^2\ g^{-1}$, 7.86 ± 3.60 $m^2\ g^{-1}$, 7.78 ± 2.98 $m^2\ g^{-1}$, and 7.96 ± 2.29 $m^2\ g^{-1}$ for winter, spring, summer, and autumn, respectively (Table S4). Similar behavior was noted by Zanatta et al. (2016), who did not observe any clear seasonal trend of MAC_{637} in BC at individual European background sites. The lack of seasonal trends in MAC_{eBC_660} suggests that MAC_{eBC_660} was likely influenced by other components and/or factors than those driving the seasonality in B_{abs} and MAC_{PM}, which was probably associated with locally emitted carbonaceous aerosols.

In this study, a seasonal variation of MAC_{eBC} appears at the 370 nm wavelength (Fig. 6e) with the mean value varying between 11.85 ± 4.67 $m^2\ g^{-1}$ in summer and 15.64 ± 4.67 $m^2\ g^{-1}$ winter (Table S4). This relatively higher MAC_{eBC_370} observed in winter could be partly a result of the influence of wood burning during the heating season. This result suggests that at the rural background site, the influence of BB is more visible on B_{abs} and MAC_{PM} than on MAC_{eBC}, especially at 660 nm.

3.3. Contribution of BrC coatings on absorption coefficient

If $\Delta\alpha\_\lambda$ is plotted as a function of $\alpha_{\_660/880}$ for the Mie-calculations and aethalometer measurements, the contribution of components in

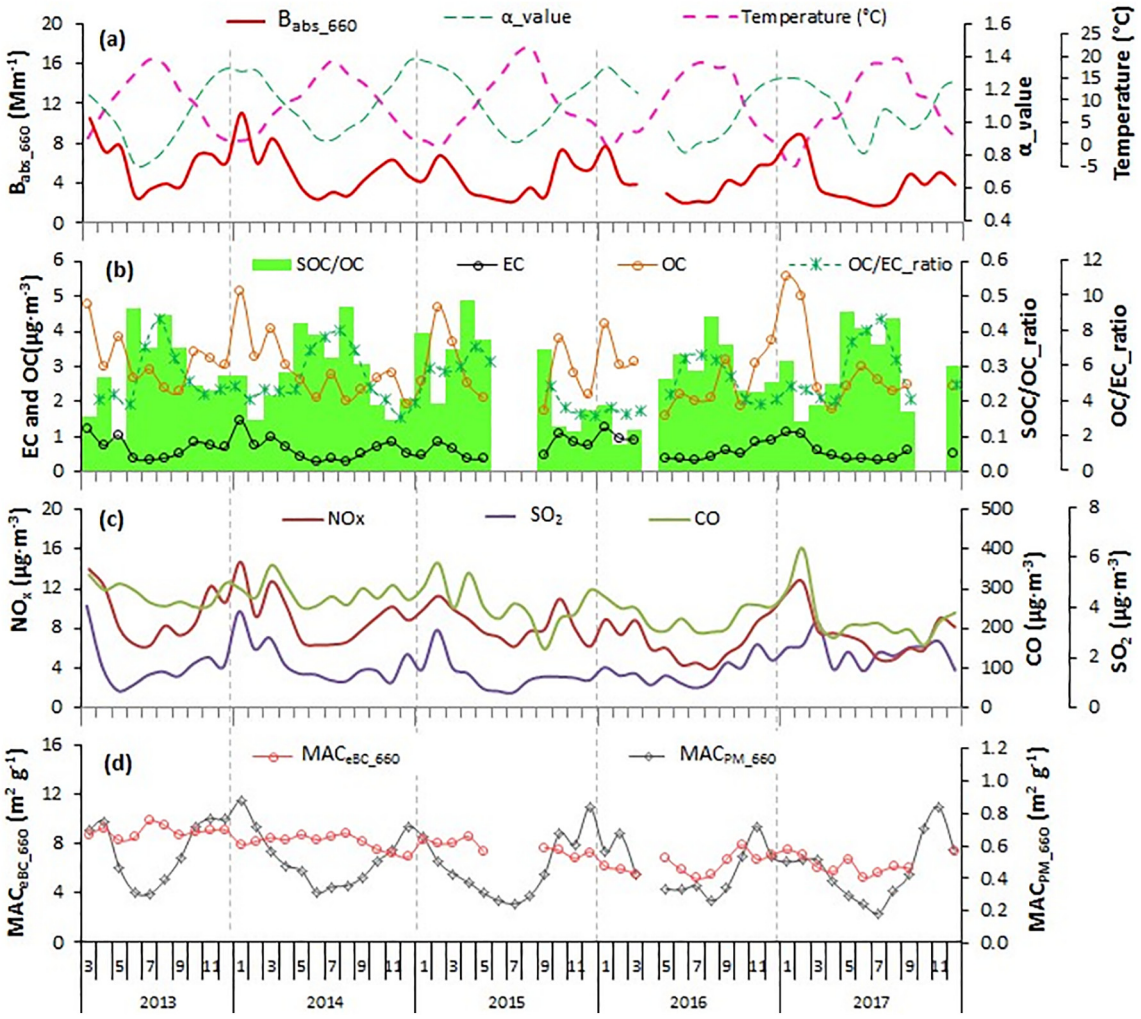

Fig. 5. Monthly mean values for (a) B_{abs_660}, α (370/880) and ambient temperature, (b) EC, OC concentrations and SOC/OC and OC/EC ratios, (c) NO_x, SO_2, CO concentrations, and (d) MAC_{eBC_660} and MAC_{PM_660}.

the sample other than BC can be estimated (Fig. 7) (Fig. S6). In Fig. 7, the Δα_λ values falling above the Mie-calculated BC region suggest the presence of components with higher absorption at shorter wavelengths (370 nm) than at longer wavelengths (660 and 880 nm) in the samples (Wang et al., 2016). The Δα_λ analysis showed that the proportion of samples with a BrC absorption (above the Mie-simulated Δα_λ range) represents 31% of the samples collected during the entire measurement period and 20%, 32%, 45%, and 28% during winter, spring, summer, and autumn, respectively (Fig. S6). The presence of BrC can be attributed to the influence of BB emissions in winter and/or the formation of secondary organic aerosols, especially during summer. The higher proportion of samples with BrC absorption can lead to absorption enhancement, as discussed in Section 3.4.

The BrC-attributed absorption at 370 nm estimated with the adoption of α = 1 ($\boldsymbol{B_{abs370\_BrC\_\alpha1}}$) was compared to the estimate with an average α of 0.5 to1.3 obtained from the lowest and the highest **Δα_λ** ($\mathbf{B_{abs370\_BrC\_\Delta\alpha\_\lambda}}$) (Wang et al., 2016). The estimated $\mathbf{B_{abs370\_BrC\_\alpha1}}$ values agreed reasonably with the median of the lowest and highest $\boldsymbol{B_{abs370\_BrC\_\Delta\alpha\_\lambda}}$ (Table **2**). The overall mean $\boldsymbol{B_{abs370\_BrC\_\alpha1}}$ was 2.10 Mm^{-1} and $\mathbf{B_{abs370\_BrC\_\Delta\alpha\_\lambda}}$ ranged from 0.70 Mm^{-1} to 3.35 Mm^{-1}. The BrC-attributed absorption at 370 nm was higher in winter ($B_{abs\_370\_BrC\_\alpha1}$ = 2.62 Mm^{-1} and $\mathbf{B_{abs370_BrC_\Delta\alpha_\lambda}}$of 0.83 to 5.02 Mm^{-1}) and lower in summer ($B_{abs\_370\_BrC\_\alpha1}$ = 0.77 Mm^{-1} and $\mathbf{B_{abs370\_BrC\_\Delta\alpha\_\lambda}}$ of 0.65 to 1.57 Mm^{-1}). The higher BrC-attributed absorption at 370 nm is consistent with the increased contribution of BB during the heating season and, therefore, with the higher α observed during this period.

The overall relative contribution of $B_{abs370\_BrC\_\alpha1}$ was 16% of the total absorption and ranged from 12% in summer to 19% in winter. Similar values (12%–19%) were reported by Li et al. (2018) at a rural site in China. The $B_{abs370_BrC_\alpha1}$values were lower than the estimated $\mathbf{B_{abs370\_BrC\_\Delta\alpha\_\lambda}}$ values, ranging from 13% to 41%. The contribution of $\mathbf{B_{abs370_BrC_\Delta\alpha_\lambda}}$observed in this study is consistent with Wang et al. (2016) using multiwavelength absorption aerosol optical depth (AAOD) observations from the AERONET network and ambient measurements of absorption with aethalometers at different sites. These authors measured the global contribution of BrC as up to 40% of the total absorption in the UV spectra, ranging from 10% to 30% at most sites. During a year-long measurement campaign at a suburban site in Nanjing (China), Leskinen et al. (2020) found that 25.3% of the samples with non-BC absorbers contributed to 27% of the total absorption.

3.4. Absorption enhancement factor (E_{abs})

Atmospheric aerosols can undergo different transformation and transport patterns, which may result in enhanced light absorption. During the 5-year measurement campaign, the overall mean E_{abs_660} was 1.35 0.46. A seasonal variation in E_{abs_660} was observed, with a maximum reached in August (Fig. 8). The mean E_{abs_660} were 1.18 ± 0.27, 1.16 ± 0.34, 1.59 ± 0.60 and 1.41 ± 0.42 for winter, spring, summer,

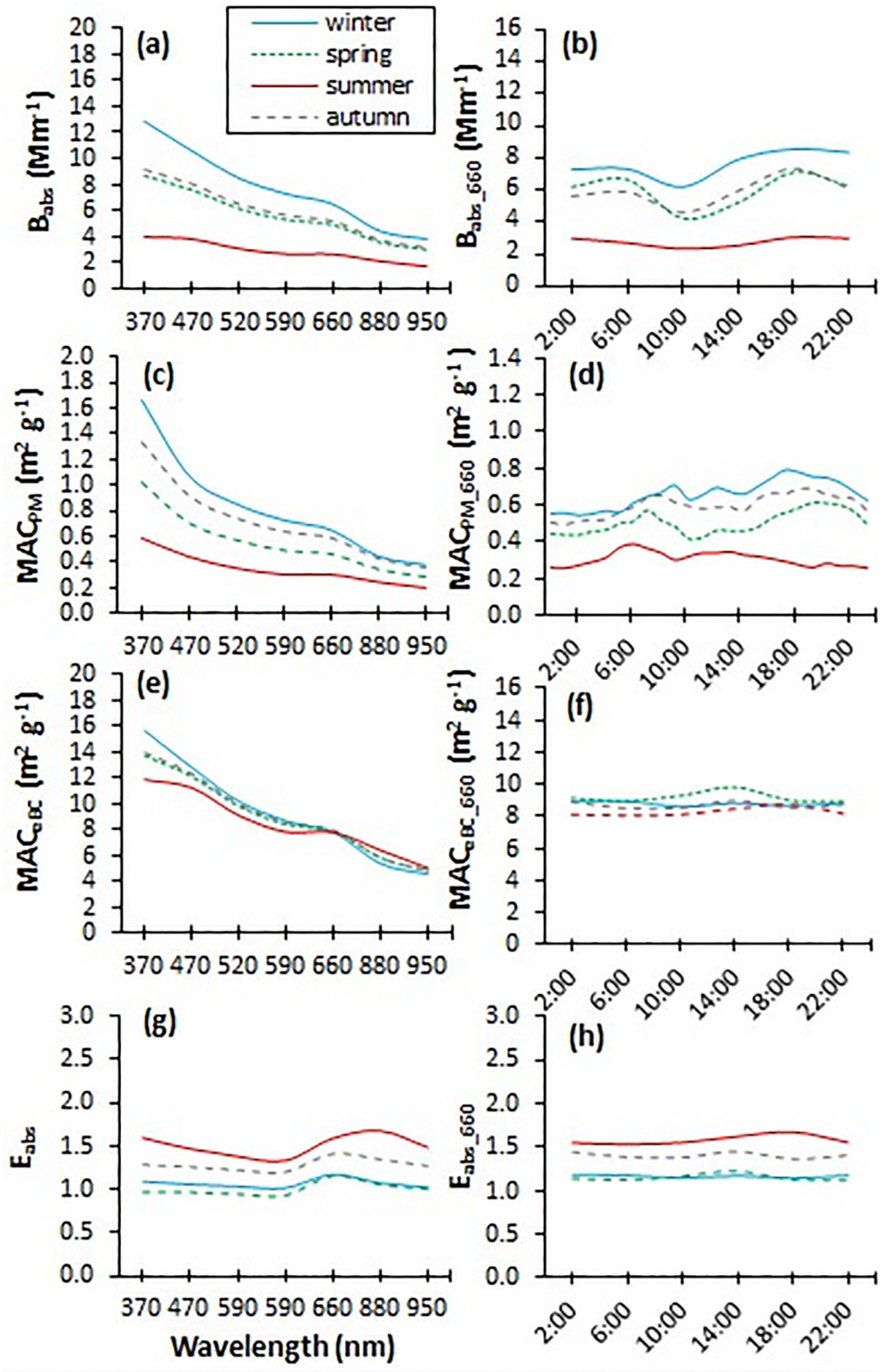

Fig. 6. Seasonal variations of a) B_{abs}, c) MAC_{PM}, e) MAC_{eBC}, and g) E_{abs} for different wavelengths and diurnal trends at 660 nm (b, d, f and h).

and autumn, respectively. The E_{abs} values reported in the literature vary depending on the emission source, physicochemical properties of the primary aerosols, and atmospheric aging (Sun et al., 2020; Wu et al., 2018). The E_{abs_660} values estimated in this study are comparable to those reported at 870 nm during the winter campaign at a Central European rural background site (Melpitz, Germany) by Yuan et al. (2020) using two different methods (1.0 1.6 or 1.2 1.9). Wu et al. (2018) reported an annual mean E_{abs_550} of 1.50 ± 0.48, in a Chinese suburban area, with the maximum value reached in August (1.97). A similar trend was observed at an urban site by Sun et al. (2020) with E_{abs_520} of 1.5 ± 0.5 in the wet season and 1.29 ± 0.28 in the dry season.

The elevated E_{abs_660} observed in summer may be partly attributed to the relatively lower MAC_{pri_660} (Fig. 8), which is sensitive to the EC concentration (Fig. S2b), but also to the influence of larger coatings

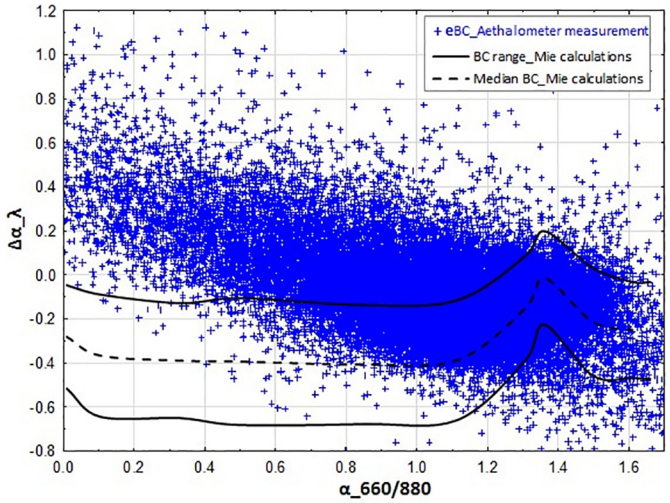

Fig. 7. Estimated Δα_λ for eBC as a function of α_660/880 based on the Mie calculations (black line) and aethalometer measurements (blue crosses) at the NAOK for the whole period. Contributions of BrC absorption is expected for the measurements lying above the upper limit (black line) of the Δα_λ for Mie calculations.

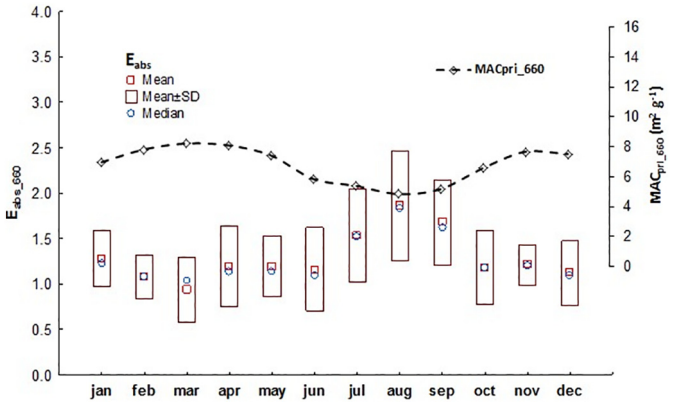

Fig. 8. Overall monthly mean and median E_{abs_660} values and mean MAC_{pri_660} measured at the NAOK.

formed on aged BC particles. While EC is chemically the same during all seasons, OC or BrC can have different formation pathways, chemical compositions, and optical properties depending on the season and transport characteristics (Lee et al., 2014). During summer, increased photochemical activity can favor the formation of internally mixed BC with secondary organic aerosols (Krasowsky et al., 2016; Schnaiter et al., 2005; Sun et al., 2020; Zhang et al., 2018). Such increased photochemical activity is consistent with the elevated OC/EC and SOC/OC ratios (Fig. 5b) and the proportionally higher fraction of samples containing BrC observed during this study (Table 2). This result is in agreement with the moderate correlation (R = 0.48) between SOC/OC ratio and B_{abs370_BrC} in summer, unlike other seasons when a weaker, or no correlation, was found (Table S5). During summer, B_{abs370_BrC} seems to be slightly peaking at noon (Fig. S7), similar to SOC and O_3 because of the maximum photochemical activity and solar radiation intensity reached at this time (Mbengue et al., 2018). Similarly, the nucleation events or days with a new particle formation (NPF) event determined according to the methodology of Dal Maso et al. (2005) were more frequent in summer (43%) than in other seasons (9%, 34%, and 14% for winter, spring, and autumn, respectively) (Table 2) (Fig. S8). The high NPF frequency suggests that BC was heavily coated with other aerosol materials in summer, and similar to Motos et al. (2020) at a high-altitude site in Switzerland.

There was neither a clear wavelength dependence of E_{abs} nor a clear diurnal variation of E_{abs_600} at NAOK (Fig. 6g, h). Therefore, local BB did not significantly affect E_{abs}, despite its higher contribution to BrC in winter. Similarly, Wu et al. (2018) and Sun et al. (2020) found a weak wavelength dependence of E_{abs} in China's suburban and urban sites. In contrast, Zhang et al. (2018) found a higher E_{abs} at 370 nm (2.25 ± 0.02) than at 880 nm (1.30 ± 0.01) in winter, which was attributed to the influence of BB at a suburban background site in Paris.

3.5. Influence of air mass origin

During the measurement period, higher B_{abs_660} and B_{abs370_BrC} values were observed under low wind speed conditions at the receptor site during winter, which was likely associated with local wood burning emissions from residential heating (Fig. S9a, b). Both B_{abs_660} and B_{abs370_BrC} also showed a higher probability of reaching over the 75th percentile of values under moderate (5–8 m s^{-1}) to strong (8–12 m s^{-1}) wind speeds from the north and the east during spring, from the northeast during winter and spring, and from the southeast during winter. The strong signal of B_{abs_660} observed during spring in the northeast wind direction was also confirmed by the PSCF analysis (Fig. 9) (S12). Apart from the spring sources in Eastern Czechia and Poland, the PSCF showed similar seasonal patterns for B_{abs_660} and B_{abs370_BrC}, with pronounced sources observed in winter over Central Europe. The most probable sources of B_{abs_660} and B_{abs370_BrC} locations were in the eastern Czech Republic and south of Poland (Silesia region). These results clearly suggest a strong relationship between B_{abs_660} and B_{abs370_BrC}, likely driven by BC sources, especially BB in winter. In Central Europe, wood burning is widely used for domestic heating (Yuan et al., 2020).

The CBPF for MAC_{eBC_660} (Fig. S9c) was comparable for all seasons, without any clear wind speed-direction dependence, except for the signal observed during summer associated with strong north and northeast winds. This result suggests that there are well-distributed sources for MAC_{eBC_660}. The sources (probabilities below 0.5) were located by the PSCF in summer over Central Europe (Czech Republic, Germany, Poland, Austria, and Switzerland) and the North Sea (Fig. 9c) (Fig. S10c). A lower probability source was also observed in autumn and spring from the south, particularly in northern Italy. The PSCF plot of MAC_{eBC} at 370 nm (Fig. S11) shows the strongest signal in winter over Czechia and neighboring countries (Slovakia, Austria, Hungry, and Germany), Northern Italy, and Northern France.

For E_{abs_660}, the highest values found during summer were associated with low to moderate wind speeds at the sampling site, mainly

Table 2
Overall and seasonal mean values of BrC-attributed absorption at 370 nm, α, Eabs_660 and nucleation events (Day of NPF).

	$B_{abs\_370\_BrC\_\alpha1}$ (Mm^{-1}, %)	$B_{abs370\_BrC\_\Delta\alpha\_\lambda}$ (Mm^{-1}, %)		α	E_{abs_660}	Days of NPF
		Min	Max			
Whole period	2.10, 16%	0.70, 14%	3.35, 39%	1.12 ± 0.23	1.35 ± 0.46	491
Winter	2.62, 19%	0.83, 14%	5.02, 41%	1.41 ± 0.13	1.18 ± 0.27	45 (9%)
Spring	1.88, 15%	0.60, 13%	3.35, 39%	1.11 ± 0.21	1.16 ± 0.34	166 (34%)
Summer	0.77, 12%	0.65, 14%	1.57, 39%	0.90 ± 0.18	1.59 ± 0.60	211 (43%)
Autumn	1.68, 13%	0.73, 15%	3.46, 38%	1.11 ± 0.18	1.41 ± 0.42	69 (14%)

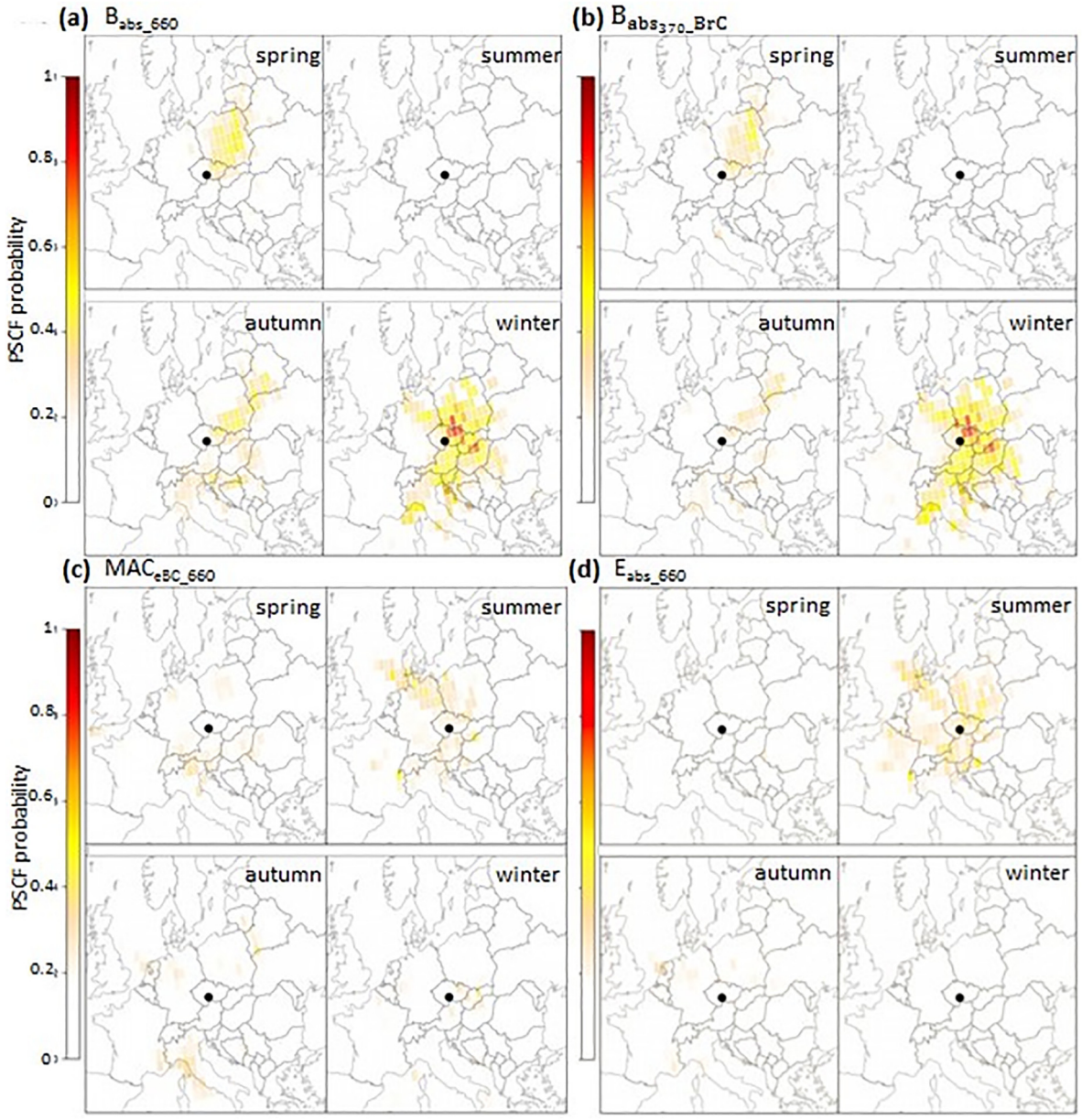

Fig. 9. The PSCF of the B_{abs_660}, $B_{abs\_370\_BrC}$, MAC_{eBC_660} and E_{abs_660} sources calculated separately for different seasons with the seasonal 75th percentile as the limit value. The location of NAOK is denoted with a black circle.

from the north and northeast (Fig. S9d). Similar to MAC_{eBC_660}, the source location was identified in summer by PSFC (Fig. 9d) and gridded back trajectory frequencies (Fig. S10d), showing the sources of high E_{abs_660} values distributed over Central Europe, mainly in August (Fig. S12), when a higher E_{abs_660} was observed (Fig. 8). In other seasons, no such pattern was observed for CBPF or PSFC. This well-distributed source of E_{abs_660} suggests that secondary aerosols formed during photochemical activity are the main source of E_{abs_660} in summer. The relatively comparable source profiles of MAC_{eBC_660} and E_{abs_660} for different seasons support the light-absorbing coating formed during atmospheric aging as the major driver of MAC_{eBC} at the rural background site.

4. Conclusion

This study investigated the absorption properties of eBC during long-term measurements at the Central European rural background site of NAOK. The MAC_{eBC} was estimated using B_{abs} measured by a multiwavelength aethalometer and EC measured by the thermo-optical method. The MAC enhancement factor (E_{abs}) was estimated by applying the MRS in the EC tracer method, and the influence of BrC on the light absorption coefficient was explored by combining different methods applicable for long-term field campaigns.

The annual mean B_{abs}, MAC_{PM}, and MAC_{eBC} measured at NAOK slightly decreased during the 5-year measurement period, which can be related to changes in size distribution in the submicron aerosol. The B_{abs} and MAC_{PM} exhibited clear seasonal and diurnal trends at all wavelengths, with the mean values doubling in winter compared to summer, likely associated with the significant contribution of BB (50%) to the total eBC observed at NAOK during the heating season (Mbengue et al., 2020). BrC was detected in 31% of the samples collected during the entire measurement period, and BrC-attributed absorption can contribute up to 40% of the total absorption measured at 370 nm at the rural background site. In contrast, MAC_{eBC} did not have a distinct temporal trend at the near-infrared wavelength, suggesting the influence of factors other than those affecting B_{abs} and MAC_{PM} seasonality,

probably local combustion sources. MAC_{eBC} exhibited a seasonal variation at shorter wavelengths (370 nm), where the influence of BrC from BB was more visible. During winter, the mean E_{abs_660} was 1.18 ± 0.27, and there was no clear wavelength dependence, despite the influence of BB emissions. The E_{abs_660} increased to 1.59 ± 0.60 in summer, likely due to BC coating by secondary aerosol fractions formed during an atmospheric aging of particles transported over Central Europe.

The comparable source location estimation (CBPF or PSFC) of MAC_{eBC_660} and E_{abs_660} supports the light-absorbing coating materials (especially BrC) formed during atmospheric aging as a major driver of the MAC_{eBC_660} measured at the regional background site. However, further field investigations of the composition of the coating materials and the mixing state of the BC particles are needed to better characterize the light absorption properties and to understand uncertainties related to the estimation of BC radiative impacts.

Data availability

The eBC, B_{abs}, OC and EC data presented in this study are available from the corresponding author upon request and can also be downloaded from the EBAS database (http://ebas.nilu.no/).

CRediT authorship contribution statement

Saliou Mbengue: Investigation, Data curation, Formal analysis, Visualization, Conceptualization, Writing – original draft. **Nadezda Zikova:** Methodology, Investigation, Formal analysis, Visualization, Conceptualization, Writing – original draft. **Jaroslav Schwarz:** Methodology, Investigation, Conceptualization, Writing – review & editing. **Petr Vodička:** Methodology, Investigation, Conceptualization, Writing – review & editing. **Adéla Holubová Šmejkalová:** Investigation, Data curation, Writing – review & editing. **Ivan Holoubek:** Project administration, Funding acquisition, Supervision, Writing – review & editing.

Declaration of competing interest

The authors declare that they have no known competing financial interests or personal relationships that could have appeared to influence the work reported in this paper.

Acknowledgements

This work has received funding from the European Union's Horizon 2020 research and innovation program under grant agreement No. 654109, European Union; and from the project for the support of national research infrastructure ACTRIS participation of the Czech Republic (ACTRIS-CZ - LM2015037 and ACTRIS-CZ LM201822) supported by the Ministry of Education, Youth and Sports of the Czech Republic (MEYS) within the National Sustainability Program I (NPU I), grant number LO1415. The work was also supported from the European Regional Development Fund-Project "ACTRIS-CZ RI" (No. CZ.02.1.01/0.0/0.0/16_013/0001315), "ACTRIS-CZ RI 2" (No. CZ.02.1.01/0.0/0.0/18_046/0015968), and MEYS's INTER-EXCELENCE INTERCOST program under grant agreements No. LTC18068. The authors gratefully acknowledge the NOAA Air Resources Laboratory (ARL) for the provision of the HYSPLIT transport and dispersion model used in this publication. The authors are also grateful to Dr. Cheng Wu (https://sites.google.com/site/wuchengust) for developing and facilitating the accessibility for different computer programs used in this work.

Appendix A. Supplementary data

Supplementary data to this article can be found online at https://doi.org/10.1016/j.scitotenv.2021.148365.

References

Andreae, M.O., Gelencsér, A., 2006. Black Carbon or Brown Carbon? The Nature of Light-absorbing Carbonaceous Aerosols.

Arnott, W.P., Hamasha, K., Moosmüller, H., Sheridan, P.J., Ogren, J.A., 2005. Towards aerosol light-absorption measurements with a 7-wavelength aethalometer: evaluation with a photoacoustic instrument and 3-wavelength nephelometer. Aerosol Sci. Technol. 39, 17–29. https://doi.org/10.1080/027868290901972.

Baumgardner, D., Avallone, L., Bansemer, A., Borrmann, S., Brown, P., Bundke, U., Chuang, P.Y., Cziczo, D., Field, P., Gallagher, M., Gayet, J.F., Heymsfield, A., Korolev, A., Krámer, M., McFarquhar, G., Mertes, S., Möhler, O., Lance, S., Lawson, P., Petters, D., Pratt, K., Roberts, G., Rogers, D., Stetzer, O., Stith, J., Strapp, W., Twohy, C., Wendisch, M., 2012. In situ, airborne instrumentation: addressing and solving measurement problems in ice clouds. Bull. Am. Meteorol. Soc. 93, 29–34. https://doi.org/10.1175/BAMS-D-11-00123.1.

Bond, T.C., Bergstrom, R.W., 2006. Light absorption by carbonaceous particles: an investigative review. Aerosol Sci. Technol. 40, 27–67. https://doi.org/10.1080/02786820500421521.

Bond, T.C., Doherty, S.J., Fahey, D.W., Forster, P.M., Berntsen, T., DeAngelo, B.J., Flanner, M.G., Ghan, S., Kärcher, B., Koch, D., Kinne, S., Kondo, Y., Quinn, P.K., Sarofim, M.C., Schultz, M.G., Schulz, M., Venkataraman, C., Zhang, H., Zhang, S., Bellouin, N., Guttikunda, S.K., Hopke, P.K., Jacobson, M.Z., Kaiser, J.W., Klimont, Z., Lohmann, U., Schwarz, J.P., Shindell, D., Storelvmo, T., Warren, S.G., Zender, C.S., 2013. Bounding the role of black carbon in the climate system: a scientific assessment. J. Geophys. Res. Atmos. 118, 5380–5552. https://doi.org/10.1002/jgrd.50171.

Cabada, J.C., Pandis, S.N., Subramanian, R., Robinson, A.L., Polidori, A., Turpin, B., 2004. Estimating the secondary organic aerosol contribution to PM2. 5 using the EC tracer method special issue of aerosol science and technology on findings from the fine particulate matter supersites program. Aerosol Sci. Technol. 38, 140–155.

Cappa, C.D., Zhang, X., Russell, L.M., Collier, S., Lee, A.K.Y., Chen, C.-L., Betha, R., Chen, S., Liu, J., Price, D.J., et al., 2019. Light absorption by ambient black and brown carbon and its dependence on black carbon coating state for two California, USA, cities in winter and summer. J. Geophys. Res. Atmos. 124, 1550–1577.

Carslaw, D.C., Ropkins, K., 2012. openair – an R package for air quality data analysis. Environ. Model. Softw. 27–28, 52–61. https://doi.org/10.1016/j.envsoft.2011.09.008.

Castro, L.M., Pio, C.A., Harrison, R.M., Smith, D.J.T., 1999. Carbonaceous aerosol in urban and rural European atmospheres: estimation of secondary organic carbon concentrations. Atmos. Environ. 33, 2771–2781.

Cavalli, F., Viana, M., Yttri, K.E., Genberg, J., Putaud, J.P., 2010. Toward a standardized thermal-optical protocol for measuring atmospheric organic and elemental carbon: the EUSAAR protocol. Atmos. Meas. Tech. 3, 79–89. https://doi.org/10.5194/amtd-2-2321-2009.

Cheng, Y., He, K.B., Zheng, M., Duan, F.K., Du, Z.Y., Ma, Y.L., Tan, J.H., Yang, F.M., Liu, J.M., Zhang, X.L., Weber, R.J., Bergin, M.H., Russell, A.G., 2011. Mass absorption efficiency of elemental carbon and water-soluble organic carbon in Beijing, China. Atmos. Chem. Phys. 11, 11497–11510. https://doi.org/10.5194/acp-11-11497-2011.

Cheng, Y., He, K. bin, Engling, G., Weber, R., Liu, J. meng, Du, Z. yu, Dong, S. ping, 2017. Brown and black carbon in Beijing aerosol: implications for the effects of brown coating on light absorption by black carbon. Sci. Total Environ. 599–600, 1047–1055. https://doi.org/10.1016/j.scitotenv.2017.05.061.

Cheng, Z., Atwi, K., El Hajj, O., Ijeli, I., Al Fischer, D., Smith, G., Saleh, R., 2021. Discrepancies between brown carbon light-absorption properties retrieved from online and offline measurements. Aerosol Sci. Technol. 55, 92–103.

Cho, C., Kim, S.-W., Lee, M., Lim, S., Fang, W., Gustafsson, Ö., Andersson, A., Park, R.J., Sheridan, P.J., 2019. Observation-based estimates of the mass absorption cross-section of black and brown carbon and their contribution to aerosol light absorption in East Asia. Atmos. Environ. 212, 65–74.

Chow, J.C., Watson, J.G., Green, M.C., Wang, X., Chen, L.-W.A., Trimble, D.L., Cropper, P.M., Kohl, S.D., Gronstal, S.B., 2018. Separation of brown carbon from black carbon for IMPROVE and Chemical Speciation Network PM2. 5 samples. J. Air Waste Manage. Assoc. 68, 494–510.

Clarke, A.D., Shinozuka, Y., Kapustin, V.N., Howell, S., Huebert, B., Doherty, S., Anderson, T., Covert, D., Anderson, J., Hua, X., Moore II, K.G., McNaughton, C., Carmichael, G., Weber, R., 2004. Size distributions and mixtures of dust and black carbon aerosol in Asian outflow: Physiochemistry and optical properties. J. Geophys. Res. 109, D15S09. https://doi.org/10.1029/2003JD004378.

Collaud Coen, M., Weingartner, E., Apituley, A., Ceburnis, D., Fierz-Schmidhauser, R., Flentje, H., Henzing, J.S., Jennings, S.G., Moerman, M., Petzold, A., Schmid, O., Baltensperger, U., 2010. Minimizing light absorption measurement artifacts of the Aethalometer: evaluation of five correction algorithms. Atmos. Meas. Tech. 3, 457–474. https://doi.org/10.5194/amt-3-457-2010.

CSD, 2016. Traffic census [WWW Document]. URL. https://www.rsd.cz/wps/portal/web/Silnice-a-dalnice/Scitani-dopravy. (Accessed 8 January 2021).

CSO, 2021. Statistical Yearbook Hl. of Prague - 2020 [WWW Document]. Czech Stat. Off URL. https://www.czso.cz/csu/czso/statisticka-rocenka-hl-m-prahy-2020. (Accessed 8 January 2021).

Dal Maso, M., Kulmala, M., Riipinen, I., Wagner, R., Hussein, T., Aalto, P.P., Lehtinen, K.E.J., 2005. Formation and growth of fresh atmospheric aerosols: eight years of aerosol size distribution data from SMEAR II, Hyytiälä, Finland. Boreal Environ. Res. 10, 323–336.

Dvorská, A., Sedlák, P., Schwarz, J., Fusek, M., Hanuš, V., Vodička, P., Trusina, J., 2015. Atmospheric station Křešín u Pacova, Czech Republic – a Central European research infrastructure for studying greenhouse gases, aerosols and air quality. Adv. Sci. Res. 12, 79–83. https://doi.org/10.5194/asr-12-79-2015.

Feng, Y., Ramanathan, V., Kotamarthi, V.R., 2013. Brown carbon: a significant atmospheric absorber of solar radiation? Atmos. Chem. Phys. Discuss. 13.

Genberg, J., van der Gon, D.H.A.C., Simpson, D., Swietlicki, E., Areskoug, H., Beddows, D., Ceburnis, D., Fiebig, M., Hansson, H.-C., Harrison, R.M., et al., 2013. Light-absorbing carbon in Europe-measurement and modelling, with a focus on residential wood combustion emissions. Atmos. Chem. Phys. 13, 8719–8738.

Hansen, A.D.A., 2005. The Aethalometer–User Manual [WWW Document]. Magee Sci. Company, California, USA URL. https://www.psi.ch/sites/default/files/import/lac/ProjectAddonCatcosOperationsEN/Aethalometer_book_2005.07.02.pdf. (Accessed 8 January 2021).

Harrison, R.M., Beddows, D.C.S., Jones, A.M., Calvo, A., Alves, C., Pio, C., 2013. An evaluation of some issues regarding the use of aethalometers to measure woodsmoke concentrations. Atmos. Environ. 80, 540–548. https://doi.org/10.1016/j.atmosenv.2013.08.026.

Herich, H., Hueglin, C., Buchmann, B., 2011. A 2.5 year's source apportionment study of black carbon from wood burning and fossil fuel combustion at urban and rural sites in Switzerland. Atmos. Meas. Tech. 4, 1409.

Karanasiou, A., Panteliadis, P., Pérez, N., Minguillón, M.C., Pandolfi, M., Titos, G., Viana, M., Moreno, T., Querol, X., Alastuey, A., 2020. Evaluation of the semi-continuous OCEC analyzer performance with the EUSAAR2 protocol. Sci. Total Environ. 747, 141266.

Kirchstetter, T.W., Novakov, T., Hobbs, P.V., 2004. Evidence that the spectral dependence of light absorption by aerosols is affected by organic carbon. J. Geophys. Res. Atmos. 109.

Kirillova, E.N., Marinoni, A., Bonasoni, P., Vuillermoz, E., Facchini, M.C., Fuzzi, S., Decesari, S., 2016. Light absorption properties of brown carbon in the high Himalayas. J. Geophys. Res. Atmos. 121, 9621–9639.

Knox, A., Evans, G.J., Brook, J.R., Yao, X., Jeong, C.-H., Godri, K.J., Sabaliauskas, K., Slowik, J.G., 2009. Mass absorption cross-section of ambient black carbon aerosol in relation to chemical age. Aerosol Sci. Technol. 43, 522–532. https://doi.org/10.1080/02786820902777207.

Kondo, Y., Sahu, L., Kuwata, M., Miyazaki, Y., Takegawa, N., Moteki, N., Imaru, J., Han, S., Nakayama, T., Oanh, N.T.K., et al., 2009. Stabilization of the mass absorption cross section of black carbon for filter-based absorption photometry by the use of a heated inlet. Aerosol Sci. Technol. 43, 741–756.

Krasowsky, T.S., McMeeking, G.R., Wang, D., Sioutas, C., Ban-Weiss, G.A., 2016. Measurements of the impact of atmospheric aging on physical and optical properties of ambient black carbon particles in Los Angeles. Atmos. Environ. 142, 496–504.

Laborde, M., Crippa, M., Tritscher, T., Jurányi, Z., Decarlo, P.F., Temime-Roussel, B., Marchand, N., Eckhardt, S., Stohl, A., Baltensperger, U., et al., 2013. Black carbon physical properties and mixing state in the European megacity Paris. Atmos. Chem. Phys. 13, 5831–5856.

Lack, D.A., Langridge, J.M., 2013. On the attribution of black and brown carbon light absorption using the Ångström exponent. Atmos. Chem. Phys. 13.

Lack, D.A., Langridge, J.M., Bahreini, R., Cappa, C.D., Middlebrook, A.M., Schwarz, J.P., 2012. Brown carbon and internal mixing in biomass burning particles. Proc. Natl. Acad. Sci. 109, 14802–14807.

Lee, H.J., Aiona, P.K., Laskin, A., Laskin, J., Nizkorodov, S.A., 2014. Effect of solar radiation on the optical properties and molecular composition of laboratory proxies of atmospheric brown carbon. Environ. Sci. Technol. 48, 10217–10226.

Leskinen, A., Ruuskanen, A., Kolmonen, P., Zhao, Y., Fang, D., Wang, Q., Gu, C., Jokiniemi, J., Hirvonen, M.-R., Lehtinen, K.E.J., et al., 2020. The contribution of black carbon and non-BC absorbers to the aerosol absorption coefficient in Nanjing, China. Aerosol Air Qual. Res. 20, 590–605.

Li, S., Zhu, M., Yang, W., Tang, M., Huang, X., Yu, Y., Fang, H., Yu, X., Yu, Q., Fu, X., et al., 2018. Filter-based measurement of light absorption by brown carbon in PM2. 5 in a megacity in South China. Sci. Total Environ. 633, 1360–1369.

Liousse, C., Cachier, H., Jennings, S.G., 1993. Optical and thermal measurements of black carbon aerosol content in different environments: variation of the specific attenuation cross-section, sigma ($σ$). Atmos. Environ. A Gen. Top. 27, 1203–1211.

Mbengue, S., Fusek, M., Schwarz, J., Vodička, P., Šmejkalová, A.H., Holoubek, I., 2018. Four years of highly time resolved measurements of elemental and organic carbon at a rural background site in Central Europe. Atmos. Environ. 182, 335–346.

Mbengue, S., Serfozo, N., Schwarz, J., Ziková, N., Šmejkalová, A.H., Holoubek, I., 2020. Characterization of equivalent black carbon at a regional background site in Central Europe: variability and source apportionment☆. Environ. Pollut. 260. https://doi.org/10.1016/j.envpol.2019.113771.

Motos, G., Corbin, J.C., Schmale, J., Modini, R.L., Bertò, M., Kupiszewski, P., Baltensperger, U., Gysel-Beer, M., 2020. Black carbon aerosols in the lower free troposphere are heavily coated in summer but largely uncoated in winter at Jungfraujoch in the Swiss Alps. Geophys. Res. Lett. 47, e2020GL088011.

Müller, T., Henzing, J.S., de Leeuw, G., Wiedensohler, A., Alastuey, A., Angelov, H., Bizjak, M., Collaud Coen, M., Engström, J.E., Gruening, C., Hillamo, R., Hoffer, A., Imre, K., Ivanow, P., Jennings, G., Sun, J.Y., Kalivitis, N., Karlsson, H., Komppula, M., Laj, P., Li, S.-M., Lunder, C., Marinoni, A., Martins dos Santos, S., Moerman, M., Nowak, A., Ogren, J.A., Petzold, A., Pichon, J.M., Rodriquez, S., Sharma, S., Sheridan, P.J., Teinilä, K., Tuch, T., Viana, M., Virkkula, A., Weingartner, E., Wilhelm, R., Wang, Y.Q., 2011. Characterization and intercomparison of aerosol absorption photometers: result of two intercomparison workshops. Atmos. Meas. Tech. 4, 245–268. https://doi.org/10.5194/amt-4-245-2011.

Nordmann, S., Birmili, W., Weinhold, K., Müller, K., Spindler, G., Wiedensohler, A., 2013. Measurements of the mass absorption cross section of atmospheric soot particles using Raman spectroscopy. J. Geophys. Res. Atmos. 118, 12–75.

Pandolfi, M., Cusack, M., Alastuey, A., Querol, X., 2011. Variability of aerosol optical properties in the Western Mediterranean Basin. Atmos. Chem. Phys. 11, 8189–8203.

Pandolfi, M., Ripoll, A., Querol, X., Alastuey, A., 2014. Climatology of Aerosol Optical Properties and Black Carbon Mass Absorption Cross Section at a Remote High-altitude Site in the Western Mediterranean Basin.

Petzold, A., Ogren, J.A., Fiebig, M., Laj, P., Li, S.M., Baltensperger, U., Holzer-Popp, T., Kinne, S., Pappalardo, G., Sugimoto, N., Wehrli, C., Wiedensohler, A., Zhang, X.Y., 2013. Recommendations for reporting black carbon measurements. Atmos. Chem. Phys. 13, 8365–8379. https://doi.org/10.5194/acp-13-8365-2013.

Pileci, R.E., Modini, R.L., Bertò, M., Yuan, J., Corbin, J.C., et al., 2021. Comparison of co-located refractory black carbon (rBC) andelemental carbon (EC) mass concentration measurements duringfield campaigns at several European sites. Atmos. Meas. Tech. 14, 1379–1403.

Pio, C., Cerqueira, M., Harrison, R.M., Nunes, T., Mirante, F., Alves, C., Oliveira, C., Sanchez de la Campa, A., Artíñano, B., Matos, M., 2011. OC/EC ratio observations in Europe: re-thinking the approach for apportionment between primary and secondary organic carbon. Atmos. Environ. 45, 6121–6132. https://doi.org/10.1016/j.atmosenv.2011.08.045.

Putaud, J.P., Raes, F., Van Dingenen, R., Brüggemann, E., Facchini, M.C., Decesari, S., Fuzzi, S., Gehrig, R., Hüglin, C., Laj, P., Lorbeer, G., Maenhaut, W., Mihalopoulos, N., Müller, K., Querol, X., Rodriguez, S., Schneider, J., Spindler, G., Ten Brink, H., Tørseth, K., Wiedensohler, A., 2004. A European aerosol phenomenology - 2: chemical characteristics of particulate matter at kerbside, urban, rural and background sites in Europe. Atmos. Environ. 38, 2579–2595. https://doi.org/10.1016/j.atmosenv.2004.01.041.

R Core Team, 2020. R: A Language and Environment for Statistical Computing [WWW Document]. URL. https://www.r-project.org/.

Rolph, G., Stein, A., Stunder, B., 2017. Real-time Environmental Applications and Display sYstem: READY. Environ. Model. Softw. 95, 210–228. https://doi.org/10.1016/j.envsoft.2017.06.025.

Sandradewi, J., Prévôt, A.S.H., Szidat, S., Perron, N., Alfarra, M.R., Lanz, V.A., Weingartner, E., Baltensperger, U.R.S., 2008. Using aerosol light abosrption measurements for the quantitative determination of wood burning and traffic emission contribution to particulate matter. Environ. Sci. Technol. 42, 3316–3323. https://doi.org/10.1021/es702253m.

Schmid, O., Artaxo, P., Arnott, W.P., Chand, D., Gatti, L.V., Frank, G.P., Hoffer, A., Schnaiter, M., Andreae, M.O., 2006. Spectral light absorption by ambient aerosols influenced by biomass burning in the Amazon Basin – I. Comparison and field calibration of absorption measurement techniques. Atmos. Chem. Phys. 6, 3443–3462. https://doi.org/10.5194/acpd-5-9355-2005.

Schnaiter, M., Linke, C., Möhler, O., Naumann, K.H., Saathoff, H., Wagner, R., Schurath, U., Wehner, B., 2005. Absorption amplification of black carbon internally mixed with secondary organic aerosol. J. Geophys. Res. D Atmos 110, 1–11. https://doi.org/10.1029/2005JD006046.

Schwarz, J., Cusack, M., Karban, J., Chalupníčková, E., Havránek, V., Smolík, J., Ždímal, V., 2016. PM2. 5 chemical composition at a rural background site in Central Europe, including correlation and air mass back trajectory analysis. Atmos. Res. 176, 108–120.

Stein, A.F., Draxler, R.R., Rolph, G.D., Stunder, B.J.B., Cohen, M.D., Ngan, F., 2015. NOAA's HYSPLIT atmospheric transport and dispersion modeling system. Bull. Am. Meteorol. Soc. 96, 2059–2077. https://doi.org/10.1175/BAMS-D-14-00110.1.

Strader, R., Lurmann, F., Pandis, S.N., 1999. Evaluation of secondary organic aerosol formation in winter. Atmos. Environ. 33, 4849–4863.

Sun, J.Y., Wu, C., Wu, D., Cheng, C., Li, M., Li, L., Deng, T., Yu, J.Z., Li, Y.J., Zhou, Q., et al., 2020. Amplification of black carbon light absorption induced by atmospheric aging: temporal variation at seasonal and diel scales in urban Guangzhou. Atmos. Chem. Phys. 20, 2445–2470.

Turpin, B.J., Huntzicker, J.J., 1991. Secondary formation of organic aerosol in the Los Angeles Basin: a descriptive analysis of organic and elemental carbon concentrations. Atmos. Environ. A Gen. Top. 25, 207–215.

Turpin, B.J., Huntzicker, J.J., 1995. Identification of secondary organic aerosol episodes and quantitation of primary and secondary organic aerosol concentrations during SCAQS. Atmos. Environ. 29, 3527–3544.

Turpin, B.J., Saxena, P., Andrews, E., 2000. Measuring and simulating particulate organics in the atmosphere: problems and prospects. Atmos. Environ. 34, 2983–3013.

Uria-Tellaetxe, I., Carslaw, D.C., 2014. Conditional bivariate probability function for source identification. Environ. Model. Softw. 59, 1–9. https://doi.org/10.1016/j.envsoft.2014.05.002.

Vaishya, A., Singh, P., Rastogi, S., Babu, S.S., 2017. Aerosol black carbon quantification in the central Indo-Gangetic Plain: seasonal heterogeneity and source apportionment. Atmos. Res. 185, 13–21.

Virkkula, A., Mäkelä, T., Hillamo, R., Yli-Tuomi, T., Hirsikko, A., Hämeri, K., Koponen, I.K., 2007. A simple procedure for correcting loading effects of aethalometer data. J. Air Waste Manage. Assoc. 57, 1214–1222. https://doi.org/10.3155/1047-3289.57.10.1214.

Vodička, P., Schwarz, J., Cusack, M., Ždímal, V., 2015. Detailed comparison of OC/EC aerosol at an urban and a rural Czech background site during summer and winter. Sci. Total Environ. 518–519, 424–433. https://doi.org/10.1016/j.scitotenv.2015.03.029.

Wang, X., Sedlacek, A.J., DeSá, S.S., Martin, S.T., Alexander, M.L., Alexander, M.L., Watson, T.B., Aiken, A.C., Springston, S.R., Artaxo, P., 2016. Deriving brown carbon from multi-wavelength absorption measurements: method and application to AERONET and Aethalometer observations. Atmos. Chem. Phys. 16, 12733–12752. https://doi.org/10.5194/acp-16-12733-2016.

Washenfelder, R.A., Attwood, A.R., Brock, C.A., Guo, H., Xu, L., Weber, R.J., Ng, N.L., Allen, H.M., Ayres, B.R., Baumann, K., Cohen, R.C., Draper, D.C., Duffey, K.C., Edgerton, E., Fry, J.L., Hu, W.W., Jimenez, J.L., Palm, B.B., Romer, P., Stone, E.A., Wooldridge, P.J., Brown, S.S., 2015. Biomass burning dominates brown carbon absorption in the rural southeastern United States. Geophys. Res. Lett. 42, 653–664. https://doi.org/10.1002/2014GL062444.

Weingartner, E., Saathoff, H., Schnaiter, M., Streit, N., Bitnar, B., Baltensperger, U., 2003. Absorption of light by soot particles: determination of the absorption coefficient by means of aethalometers. J. Aerosol Sci. 34, 1445–1463. https://doi.org/10.1016/S0021-8502(03)00359-8.

WMO, 2016. WMO/GAW Aerosol Measurement Procedures, Guidelines and Recommendations. 2nd edition.

Wu, C., 2017a. Minimum R Squared Method (MRS). https://doi.org/10.5281/ZENODO.832396.

Wu, C., 2017b. Mie Scattering [WWW Document]. https://doi.org/10.5281/zenodo.832400.

Wu, C., Yu, J.Z., 2016. Determination of primary combustion source organic carbon-to-elemental carbon (OC/EC) ratio using ambient OC and EC measurements: secondary OC-EC correlation minimization method. Atmos. Chem. Phys. 16, 5453–5465.

Wu, C., Wu, D., Yu, J.Z., 2018. Quantifying black carbon light absorption enhancement with a novel statistical approach. Atmos. Chem. Phys. 18, 289.

Yttri, K.E., Aas, W., Bjerke, A., Cape, J.N., Cavalli, F., Ceburnis, D., Dye, C., Emblico, L., Facchini, M.C., Forster, C., et al., 2007. Elemental and organic carbon in PM 10: a one year measurement campaign within the European Monitoring and Evaluation Programme EMEP. Atmos. Chem. Phys. 7, 5711–5725.

Yuan, J., Modini, R.L., Zanatta, M., Herber, A.B., Müller, T., Wehner, B., Poulain, L., Tuch, T., Baltensperger, U., Gysel-Beer, M., 2020. Variability in the mass absorption cross-section of black carbon (BC) aerosols is driven by BC internal mixing state at a central European background site (Melpitz, Germany) in winter. Atmos. Chem. Phys. Discuss. 1–36.

Zanatta, M., Gysel, M., Bukowiecki, N., Müller, T., Weingartner, E., Areskoug, H., Fiebig, M., Yttri, K.E., Mihalopoulos, N., Kouvarakis, G., et al., 2016. A European aerosol phenomenology-5: climatology of black carbon optical properties at 9 regional background sites across Europe. Atmos. Environ. 145, 346–364.

Zhang, Y., Favez, O., Canonaco, F., Liu, D., Močnik, G., Amodeo, T., Sciare, J., Prévôt, A.S.H., Gros, V., Albinet, A., 2018. Evidence of major secondary organic aerosol contribution to lensing effect black carbon absorption enhancement. npj Clim. Atmos. Sci. 1. https://doi.org/10.1038/s41612-018-0056-2.

Zíková, N., Ždímal, V., 2013. Long-term measurement of aerosol number size distributions at rural background station Košetice. Aerosol Air Qual. Res. 13, 1–11. https://doi.org/10.4209/aaqr.2013.02.0056.

Zíková, N., Wang, Y., Yang, F., Li, X., Tian, M., Hopke, P.K., 2016. On the source contribution to Beijing PM2.5 concentrations. Atmos. Environ. 134, 84–95. https://doi.org/10.1016/j.atmosenv.2016.03.047.